
SADDLe: Sharpness-Aware Decentralized Deep Learning with Heterogeneous Data

Sakshi Choudhary Sai Aparna Aketi Kaushik Roy
Department of Electrical and Computer Engineering
Purdue University
West Lafayette, IN 47906
{choudh23, saketi, kaushik}@purdue.edu

Abstract

Decentralized training enables learning with distributed datasets generated at different locations without relying on a central server. In realistic scenarios, the data distribution across these sparsely connected learning agents can be significantly heterogeneous, leading to local model over-fitting and poor global model generalization. Another challenge is the high communication cost of training models in such a peer-to-peer fashion without any central coordination. In this paper, we jointly tackle these two-fold practical challenges by proposing SADDLe, a set of sharpness-aware decentralized deep learning algorithms. SADDLe leverages Sharpness-Aware Minimization (SAM) to seek a flatter loss landscape during training, resulting in better model generalization as well as enhanced robustness to communication compression. We present two versions of our approach and conduct extensive experiments to show that SADDLe leads to 1-20% improvement in test accuracy compared to other existing techniques. Additionally, our proposed approach is robust to communication compression, with an average drop of only 1% in the presence of up to $4\times$ compression.

1 Introduction

Federated learning enables training with distributed data across multiple agents under the orchestration of a central server [29]. However, the presence of such a central entity can lead to a single point of failure and network bandwidth issues [6]. To address these concerns, several decentralized learning algorithms have been proposed [33, 6, 2, 13, 34, 1, 28]. Decentralized learning is a peer-to-peer learning paradigm in which agents connected in a fixed graph topology learn by communicating with their peers/neighbors without the need for a central server. The authors in [33] present Decentralized Parallel Stochastic Gradient Descent (DPSGD), which combines SGD with gossip averaging algorithm [47] and show that the convergence rate of DPSGD is similar to its centralized counterpart [10]. Decentralized Momentum Stochastic Gradient Descent [7] introduced momentum to DPSGD, while Stochastic Gradient Push (SGP) [6] extends DPSGD to directed and time-varying graphs.

The above-mentioned algorithms assume the data to be independently and identically distributed (IID) across the agents. However, in real-world applications, the data distributions can be remarkably different, i.e. non-IID or heterogeneous [18]. While several algorithms have been proposed to mitigate the impact of such data heterogeneity [34, 2, 13, 1, 28, 44], these algorithms do not explicitly focus on the aspect of communication cost. In decentralized learning, agents communicate the models with their neighbors after every mini-batch update, leading to high communication costs. Various communication compression techniques have been proposed to address this, but these algorithms primarily focus on the settings when the data distribution is IID [26, 45, 46].

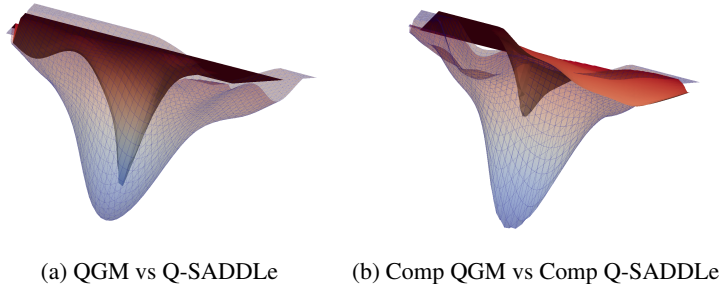


Figure 1: Loss landscape visualization for QGM (surface) vs Q-SADDLe (mesh) and Comp QGM (surface) vs Comp Q-SADDLe (mesh) for ResNet-20 trained on CIFAR-10 with non-IID data across 10 agents. Comp signifies communication compression through 8-bit stochastic quantization.

In this paper, we aim to answer the following question: *Can we improve the performance of decentralized learning on heterogeneous data in terms of test accuracy as well as communication efficiency?* We put forward an orthogonal direction of enhancing the local training at each agent to positively impact the global model generalization. We propose that seeking a flatter loss landscape during training can alleviate the issue of local over-fitting, a common concern in decentralized learning scenarios with non-IID data. To achieve this, we propose SADDLe, a set of sharpness-aware decentralized deep learning algorithms. SADDLe improves generalization by simultaneously minimizing the loss value and the sharpness through gradient perturbation. This is enabled by utilizing Sharpness-Aware Minimization (SAM) [14] to seek parameters that lie in neighborhoods with uniformly low loss values. Further, in the presence of communication compression, we find that SAM leads to lower compression error, along with enhanced robustness to compression error. Leveraging this, we demonstrate that SADDLe can be used in synergy with existing decentralized learning algorithms for non-IID data to attain better generalization and reduce the accuracy drop incurred due to compression. Specifically, we present two versions of our approach: Q-SADDLe, which incorporates a Quasi Global Momentum (QGM) buffer [34], and N-SADDLe, which utilizes cross-gradient information [2]. Figure 1 presents a visualization of the loss landscape [32] for QGM, Q-SADDLe, and their compressed counterparts. Clearly, Q-SADDLe has a much smoother loss landscape, resulting in better generalization and minimal performance loss due to communication compression. Our detailed theoretical analysis highlights that the convergence rate of Q-SADDLe matches the well-known best result in decentralized learning [33]. We also conduct extensive experiments to establish that Q-SADDLe and N-SADDLe achieve better accuracy than state-of-the-art decentralized algorithms [34, 2], with a minimal accuracy drop due to communication compression.

In summary, we make the following contributions:

- We propose Sharpness-Aware Decentralized Deep Learning (SADDLe) to seek flatter loss landscapes in decentralized learning, alleviating the local over-fitting with non-IID data.
- Leveraging the fact that flatter loss landscapes tend to be more robust to compression errors, we demonstrate that SADDLe improves communication efficiency in the presence of data heterogeneity.
- We theoretically establish that SADDLe leads to a convergence rate of $\mathcal{O}(1/\sqrt{nT})$, similar to existing decentralized learning algorithms [33].
- Through extensive experiments on various datasets, models, graphs, and compression schemes, we show that Q-SADDLe and N-SADDLe result in a 1-20% improvement in test accuracy. Additionally, our proposed algorithms maintain a minimal accuracy drop of 1% for up to $4\times$ compression, in contrast to the 4.3% average accuracy drop for the baselines.

2 Related Work

Data Heterogeneity. The impact of data heterogeneity in decentralized learning is an active area of research [34, 2, 13, 1, 28, 44]. Quasi-Global Momentum (QGM) [34] improves decentralized learning with non-IID data through a globally synchronized momentum buffer. Gradient Tracking [28] tracks average gradients but requires 2x communication overhead as compared to DPSGD [33],

while Global Update Tracking [1] tracks the average model updates to enhance performance with heterogeneous data. Cross Gradient Aggregation (CGA) [13] and Neighborhood Gradient Mean (NGM) [2] utilize cross-gradient information through an extra communication round, achieving state-of-the-art performance in terms of test accuracy. In this work, we take an orthogonal route and focus on improving local training with a flatness-seeking optimizer [14] to achieve better generalization.

Communication Compression. Several algorithms have been proposed for communication-restricted decentralized settings [43, 45, 26, 48]. DeepSqueeze [45] introduced error-compensated compression to decentralized learning. Choco-SGD [26] communicates compressed model updates rather than parameters and achieves better accuracy than DeepSqueeze. Recently, BEER [48] adopted communication compression with gradient tracking [28], resulting in a faster convergence rate than Choco-SGD [26]. However, as shown in QGM [34], gradient tracking doesn’t scale well for deep learning models and requires further study. In this paper, we compress the first (and only) communication round in Q-SADDLe and the second round in N-SADDLe. In both cases, we observe that SADDLe aids communication efficiency by alleviating the severe accuracy degradation incurred due to compression in existing decentralized learning algorithms for non-IID data [34, 2].

Sharpness-Aware Minimization. Sharpness-Aware Minimization (SAM) [14] explores the connection between the flatness of minima and generalization by simultaneously minimizing loss value and loss sharpness during training [25, 23]. The authors in [5] provide a theoretical understanding of SAM through convergence results. Several variants of SAM have been proposed for centralized learning [49, 31, 36, 12, 22, 37]. In addition, there have been several efforts to improve the generalization performance in federated learning using SAM [38, 8, 42, 9]. Recently, DFedSAM [40] was proposed to improve the model consistency in decentralized federated learning settings, where agents communicate with each other after multiple local iterations. In contrast, our work focuses on simultaneously improving test accuracy and communication efficiency for decentralized learning with extreme data heterogeneity where agents communicate after every local iteration.

3 Background

A global model is learned in decentralized learning by aggregating models trained on locally stored data at n agents connected in a sparse graph topology. This topology is modeled as a graph $G = ([n], \mathbf{W})$, where \mathbf{W} is the mixing matrix indicating the graph’s connectivity. Each entry w_{ij} in \mathbf{W} encodes the effect of agent j on agent i , and $w_{ij} = 0$ implies that agents i and j are not connected directly. $\mathcal{N}(i)$ represents neighbors of i including itself. We aim to minimize the global loss function $f(\mathbf{x})$ shown in equation 1. Here, $F_i(\mathbf{x}; d_i)$ is the local loss function at agent i , and $f_i(\mathbf{x})$ is the expected value of $F_i(\mathbf{x}; d_i)$ over the dataset D_i .

$$\min_{\mathbf{x} \in \mathbb{R}^d} f(\mathbf{x}) = \frac{1}{n} \sum_{i=1}^n f_i(\mathbf{x}), \text{ where } f_i(\mathbf{x}) = \mathbb{E}_{d_i \sim D_i} [F_i(\mathbf{x}; d_i)] \quad \forall i \quad (1)$$

DPSGD[33] tackles this by combining Stochastic Gradient Descent (SGD) with gossip averaging algorithms [47]. Each agent maintains model parameters \mathbf{x}_i^t , computes local gradient \mathbf{g}_i^t through SGD, and incorporates neighborhood information as shown in the following update rule:

$$\text{DPSGD: } \mathbf{x}_i^{t+1} = \sum_{j \in \mathcal{N}(i)} w_{ij} \mathbf{x}_j^t - \eta \mathbf{g}_i^t; \quad \mathbf{g}_j^t = \nabla F_j(\mathbf{x}_j^t, d_j^t). \quad (2)$$

DPSGD assumes the data distribution across the agents to be IID and results in significant performance degradation in the presence of data heterogeneity. To handle this, QGM [34] incorporates a globally synchronized momentum buffer within DPSGD. This mitigates the impact of non-IID data by maintaining a form of global information through the momentum buffer, resulting in better test accuracy without any extra communication overhead. To further improve the performance with extreme heterogeneity, NGM[2] and CGA[13] utilize cross-gradients obtained through an additional communication round. In the first communication round, the agents exchange models with each other (similar to DPSGD). However, in the second round, the agents communicate cross-gradients computed over the neighbors’ models and their local data. Each gradient update is a weighted average of the self and received cross-gradients [2]. Note that these algorithms represent two distinct variants proposed to enhance decentralized learning with non-IID data based on the available communication budget. Additional details are presented in Appendix B.1.

4 Methodology

This section presents the two variants of SADDLe and their communication-compressed versions.

4.1 SADDLe

In the presence of data heterogeneity, models in decentralized training tend to overfit the local data at each agent. Aggregating such models adversely impacts the global model’s generalization ability. To circumvent this, we propose SADDLe, which purposely seeks a flatter loss landscape in each training iteration through Sharpness-Aware Minimization (SAM) [14]. Instead of focusing on finding parameters with low loss values like SGD, SAM searches for parameters whose neighborhoods have uniformly low loss. This is achieved by adding a perturbation ξ_i to the model parameters, which is obtained through a scaled gradient ascent step. To summarize, SADDLe aims to solve the following optimization problem:

$$f(\mathbf{x}) = \frac{1}{n} \sum_{i=1}^n \mathbb{E}_{d_i \sim D_i} \max_{\|\xi_i\| \leq \rho} [F_i(\mathbf{x}_i^t + \xi_i; d_i)] \quad \forall i, \text{ where } \xi_i = \rho \frac{\mathbf{g}_i}{\|\mathbf{g}_i\|} \quad (3)$$

Here, ρ is a tunable hyperparameter, defining the perturbation radius. Since SADDLe modifies the local optimizer at each agent, it is orthogonal to existing techniques and can be used in synergy to improve performance with non-IID data. We employ a QGM buffer [34] and cross-gradients similar to NGM [2] with SADDLe and present two versions: Q-SADDLe and N-SADDLe. The differences between QGM and Q-SADDLe are highlighted in Algorithm 1. In particular, Q-SADDLe utilizes the SAM-based gradient update $\tilde{\mathbf{g}}_i$ shown in line 4 instead of the gradient update \mathbf{g}_i . N-SADDLe employs SAM-based self and cross-gradients to further improve the performance of NGM. Algorithm 3 in the Appendix summarizes the difference in training procedures for NGM and N-SADDLe.

Algorithm 1 QGM v.s. Q-SADDLe

Input: Each agent $i \in [1, n]$ initializes model parameters \mathbf{x}_i , $\hat{\mathbf{m}}_i^{(0)} = 0$, step size η , momentum coefficients β, μ , mixing matrix $\mathbf{W} = [w_{ij}]_{i,j \in [1, n]}$, $\mathcal{N}(i)$ represents neighbors of i including itself.

procedure TRAIN() for $\forall i$

1. **for** $t = 1, 2, \dots, T$ **do**
 2. $\mathbf{g}_i^t = \nabla F_i(\mathbf{x}_i^t; d_i^t)$ for $d_i^t \sim D_i$
 3. $\mathbf{m}_i^{(t)} = \beta \hat{\mathbf{m}}_i^{(t-1)} + \mathbf{g}_i^{(t)}$
 4. $\tilde{\mathbf{g}}_i^t = \nabla F_i(\mathbf{x}_i^t + \xi(\mathbf{x}_i^t); d_i^t)$, where $\xi(\mathbf{x}_i^t) = \rho \frac{\mathbf{g}_i^t}{\|\mathbf{g}_i^t\|}$
 5. $\mathbf{m}_i^{(t)} = \beta \hat{\mathbf{m}}_i^{(t-1)} + \tilde{\mathbf{g}}_i^{(t)}$
 6. $\mathbf{x}_i^{(t+1/2)} = \mathbf{x}_i^{(t)} - \eta \mathbf{m}_i^{(t)}$
 7. SENDRECEIVE($\mathbf{x}_i^{(t+1/2)}$)
 8. $\mathbf{x}_i^{t+1} = \sum_{j \in \mathcal{N}_i^{(t)}} w_{ij} \mathbf{x}_j^{(t+1/2)}$
 9. $\mathbf{d}_i^{(t)} = \frac{\mathbf{x}_i^{(t)} - \mathbf{x}_i^{(t+1)}}{\eta}$
 10. $\hat{\mathbf{m}}_i^{(t)} = \mu \hat{\mathbf{m}}_i^{(t-1)} + (1 - \mu) \mathbf{d}_i^{(t)}$
 11. **end**
- return** \mathbf{x}_i^T
-

4.2 SADDLe with Compressed Communication

A major concern in decentralized learning is the high communication cost of training. Hence, we also investigate the impact of a flatter loss landscape on communication efficiency. We present compressed versions of QGM and Q-SADDLe in Algorithm 2. Instead of sharing models \mathbf{x}_i , the agents exchange compressed model updates \mathbf{q}_i (similar to Choco-SGD [26]). Each agent maintains compressed copies $\hat{\mathbf{x}}_j$ of their neighbors and employs a modified gossip averaging step as shown on line 7 (Algorithm 2).

Similarly, we implement Comp NGM and Comp N-SADDLe to compress the second communication round, which involves sharing cross-gradients (Algorithm 4 in Appendix). In addition to robustness to data heterogeneity, seeking flatter models also results in higher resiliency to compression error.

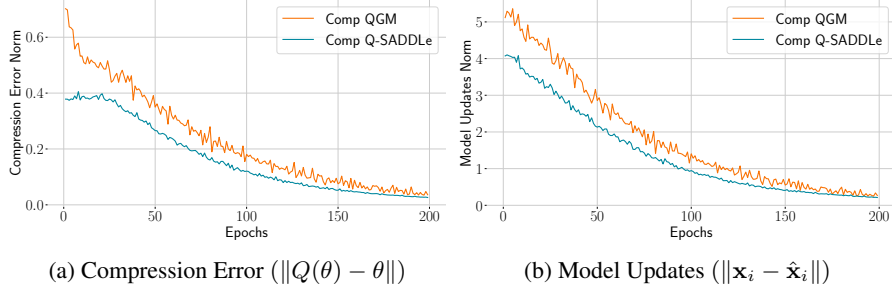


Figure 2: Impact of flatness on (a) Compression Error and (b) Model Updates for ResNet-20 trained on CIFAR-10 distributed in a non-IID manner across a 10 agent ring topology.

Interestingly, Comp Q-SADDLe and Comp N-SADDLe incur less compression error than Comp QGM and Comp NGM respectively, leading to a lower accuracy drop due to compression. We investigate this with the aid of a well-known bound on the compression error. For a compression operator $Q(\cdot)$, the expectation of error $\|Q(\theta) - \theta\|$ is bounded as:

$$\mathbb{E}_Q \|Q(\theta) - \theta\|^2 \leq (1 - \delta) \|\theta\|^2, \text{ where } \delta > 0 \quad (4)$$

In our setup, θ corresponds to model updates ($\mathbf{x}_i - \hat{\mathbf{x}}_i$) for Comp QGM and Comp Q-SADDLe, and gradients for Comp NGM and Comp N-SADDLe. Note that a wide range of compression operators (with some δ) have been shown to adhere to this bound [26, 27, 3, 4, 41]. Figure 2 shows the norm of compression error (i.e. $\|Q(\theta) - \theta\|$) and the norm of model updates (i.e. $\|\theta\| = \|\mathbf{x}_i - \hat{\mathbf{x}}_i\|$) for Comp QGM and Comp Q-SADDLe for ResNet-20 trained on CIFAR-10 in a 10 agent ring with extreme data heterogeneity. It can be observed that Q-SADDLe leads to a lower norm of model updates ($\|\theta\|$) and lower compression error. In essence, the bound in equation 4 is tighter for Q-SADDLe than QGM in the presence of compression. We observe similar trends for N-SADDLe (refer Figure 5).

Algorithm 2 Comp QGM v.s. Comp Q-SADDLe

Input: Each agent $i \in [1, n]$ initializes model parameters \mathbf{x}_i and $\hat{\mathbf{x}}_i^1 = 0$, step size η , momentum coefficients β, μ , global averaging rate γ , mixing matrix $\mathbf{W} = [w_{ij}]_{i,j \in [1,n]}$.

```

procedure TRAIN() for  $\forall i$ 
1. for  $t = 1, 2, \dots, T$  do
2.    $\mathbf{g}_i^t = \nabla F_i(\mathbf{x}_i^t; d_i^t)$  for  $d_i^t \sim D_i$ 
3.    $\mathbf{m}_i^{(t)} = \beta \hat{\mathbf{m}}_i^{(t-1)} + \mathbf{g}_i^{(t)}$ 
4.    $\tilde{\mathbf{g}}_i^t = \nabla F_i(\mathbf{x}_i^t + \xi(\mathbf{x}_i^t); d_i^t)$ , where  $\xi(\mathbf{x}_i^t) = \rho \frac{\mathbf{g}_i^t}{\|\mathbf{g}_i^t\|}$ 
5.    $\mathbf{m}_i^{(t)} = \beta \hat{\mathbf{m}}_i^{(t-1)} + \tilde{\mathbf{g}}_i^{(t)}$ 
6.    $\mathbf{x}_i^{(t+1/2)} = \mathbf{x}_i^{(t)} - \eta \mathbf{m}_i^{(t)}$ 
7.    $\mathbf{x}_i^{(t+1)} = \mathbf{x}_i^{(t+1/2)} + \gamma \sum_{j \in \mathcal{N}(i)} w_{ij} (\hat{\mathbf{x}}_j^{(t)} - \hat{\mathbf{x}}_i^{(t)})$ 
8.    $\mathbf{d}_i^{(t)} = \frac{\mathbf{x}_i^{(t)} - \mathbf{x}_i^{(t+1)}}{\eta}$ 
9.    $\hat{\mathbf{m}}^{(t)} = \mu \hat{\mathbf{m}}_i^{(t-1)} + (1 - \mu) \mathbf{d}_i^{(t)}$ 
10.   $\mathbf{q}_i^{(t)} = Q(\mathbf{x}_i^{(t+1)} - \hat{\mathbf{x}}_i^{(t)})$ 
11.  SENDRECEIVE( $\mathbf{q}_i^{(t)}$ )
12.   $\hat{\mathbf{x}}_j^{(t+1)} = \mathbf{q}_j^{(t)} + \hat{\mathbf{x}}_j^{(t)}$  for all  $j \in \mathcal{N}(i)$ 
13. end
return  $\mathbf{x}_i^T$ 

```

5 Convergence Rate Analysis

In this section, we provide a convergence analysis for Q-SADDLe. Similar to prior works in decentralized learning [33, 34], we make the following standard assumptions:

Assumption 1 - Lipschitz Gradients: Each function $f_i(\mathbf{x})$ is L -smooth i.e., $\|\nabla f_i(\mathbf{y}) - \nabla f_i(\mathbf{x})\| \leq L\|\mathbf{y} - \mathbf{x}\|$.

Assumption 2 - Bounded Variance: The variance of the stochastic gradients is assumed to be bounded. There exist constants σ and δ such that

$$\mathbb{E}_{d \sim \mathcal{D}_i} \|\nabla F_i(\mathbf{x}; d) - \nabla f_i(\mathbf{x})\|^2 \leq \sigma^2; \frac{1}{n} \sum_{i=1}^n \|\nabla f_i(\mathbf{x}) - \nabla f(\mathbf{x})\|^2 \leq \delta^2 \quad \forall i \quad (5)$$

Assumption 3 - Doubly Stochastic Mixing Matrix: \mathbf{W} is a real doubly stochastic matrix which satisfies $\mathbb{E}_{\mathbf{W}} \|\mathbf{Z}\mathbf{W} - \bar{\mathbf{Z}}\|^2 \leq (1 - \lambda) \|\mathbf{Z} - \bar{\mathbf{Z}}\|^2$ for any matrix $\mathbf{Z} \in \mathbb{R}^{d \times n}$ and $\bar{\mathbf{Z}} = \mathbf{Z} \frac{1}{n} \mathbf{1}^T$.

Theorem 1 presents convergence of the proposed Q-SADDLe algorithm (proof in Appendix A.1).

Theorem 1 *Given Assumptions 1-3, for a momentum coefficients β and μ , let the learning rate satisfy $\eta \leq \min\left(\frac{\lambda}{7L}, \frac{1-\beta}{4L}, \frac{(1-\beta)^2(1-\mu)}{\sqrt{12}L\beta}\right)$. For all $T \geq 1$, we have*

$$\begin{aligned} \frac{1}{T} \sum_{t=0}^{T-1} \mathbb{E} \left[\|\nabla f(\bar{\mathbf{x}}_t)\|^2 \right] &\leq \frac{4}{\tilde{\eta}T} (\mathbb{E}[f(\bar{x}^0) - f^*]) + \left(\frac{6\tilde{\eta}L}{n} + 18\tilde{\eta}^2 L^2 C_2 + \frac{768\tilde{\eta}^2 L^2 C_1}{\lambda^2} \right) \sigma^2 \\ &+ \left(\frac{832L^2 \tilde{\eta}^2 (1-\beta)^2}{\lambda^2} \right) \delta^2 + \left(8L^2 + \frac{12\tilde{\eta}L^3}{n} + 36\tilde{\eta}^2 L^4 C_2 + \frac{3136L^4 \tilde{\eta}^2 C_1}{\lambda^2} \right) \rho^2 \end{aligned} \quad (6)$$

where $C_1 = \frac{(2-\beta-\mu)(1-\beta)^2}{(1-\mu)}$, $C_2 = \frac{\beta^2}{(1-\mu)(1-\beta)}$, \bar{x} is the average/consensus model and $\tilde{\eta} = \frac{\eta}{(1-\beta)}$.

We observe that the convergence rate includes three main terms related to the suboptimality gap $f(\bar{x}^0) - f^*$, the sampling variance σ and the gradient variance δ representing data heterogeneity, followed by an additional term compared to existing state-of-the-art decentralized convergence bounds [33, 34]. This term includes the perturbation radius ρ , signifying the impact of leveraging gradient perturbation to improve generalization in a decentralized learning setting. We present a corollary to show the convergence rate in terms of training iterations (proof in Appendix A.2).

Corollary 2 *Suppose that the learning rate satisfies $\eta = \mathcal{O}\left(\sqrt{\frac{\rho}{T}}\right)$ and $\rho = \mathcal{O}\left(\sqrt{\frac{1}{T}}\right)$. For a sufficiently large T ,*

$$\frac{1}{T} \sum_{t=0}^{T-1} \mathbb{E} \left[\|\nabla f(\bar{\mathbf{x}}_t)\|^2 \right] \leq \mathcal{O} \left(\frac{1}{\sqrt{nT}} + \frac{1}{T} + \frac{1}{T^{3/2}} + \frac{1}{T^2} \right) \quad (7)$$

Note that the dominant term here is $(1/\sqrt{nT})$, and the terms introduced because of the additional SGD step for flatness (i.e., $1/T^{3/2}$ and $1/T^2$) can be ignored due to their higher order. This convergence rate matches the well-known best result in existing decentralized learning algorithms [33].

6 Experiments

6.1 Experimental Setup

We analyze the test accuracy and communication efficiency of the proposed Q-SADDLe and N-SADDLe techniques and compare them with the current state-of-the-art algorithms QGM and NGM. We evaluate the proposed algorithms across diverse datasets, model architectures, graph topologies, graph sizes, and compression operators. The analysis is presented on - (a) **Datasets** (D.3): CIFAR-10 [30], CIFAR-100 [30], Imagenette [20] and ImageNet [11], (b) **Model architectures** (D.4): ResNet-20, ResNet-18 and MobileNet-v2, (c) **Graph topologies**: ring with 2 peers/agent and torus with 4 peers/agent (visualization in Figure 8), (d) **Graph sizes**: 5 to 40 agents, and (e) **Compression**

operators: Stochastic quantization [3], Top-k sparsification [4, 41] and Sign SGD [24]. For QGM, stochastic quantization diverges beyond 8-10 bits, while top-k diverges beyond 30% sparsification. We posit that this results from erroneous (compressed) updates affecting both the gossip and the momentum buffer (line 7 and 8, Algorithm 2). In contrast, the second communication round in NGM is much more compressible, as the communication compression only affects the gradient updates (line 18, Algorithm 4). Hence, for NGM and N-SADDLe, we present results for 1-bit Sign SGD.

We focus on non-IID data partitions generated through a Dirichlet distribution [19] by changing the concentration parameter α - the smaller the α , the larger the non-IIDness (refer to Figure 9). These partitions are non-overlapping, with no shuffling across the agents during training. Please refer to Appendix D.5 for details related to hyperparameters.

6.2 Results

Performance Comparison: As shown in Table 1, for CIFAR-10 Q-SADDLe results in 8.4% better accuracy on average as compared to QGM[34] across a range of graph sizes and two different degrees of non-IIDness ($\alpha = 0.01, 0.001$). QGM suffers a 1-6% accuracy drop in the presence of a stochastic quantization-based compression scheme, whereas, for Q-SADDLe, this drop is only 0-1.5%. For a challenging dataset such as CIFAR-100, Table 1 shows that Q-SADDLe outperforms QGM by $\sim 6\%$ on average. The accuracy drop due to compression is 1-8% for QGM, while Q-SADDLe proves to be more resilient to compression error with only a 0-1.8% drop in accuracy. We present additional results on Imagenette, a subset of ImageNet trained on MobileNet-v2 in Table 2. Q-SADDLe leads to an average improvement of $\sim 12\%$ over QGM, with only a 0-2% drop in accuracy due to compression. In contrast, QGM incurs a significant drop of 4-9% in the presence of communication compression. Furthermore, as the degree of non-IIDness is increased from $\alpha = 0.01$ to $\alpha = 0.001$, QGM suffers from an 8.5% average drop in accuracy, whereas Q-SADDLe nearly retains the performance. We present additional results for Top-30% Sparsification in Table 6.

Table 1: Test accuracy of QGM, Q-SADDLe, and their compressed versions evaluated on CIFAR-10 and CIFAR-100 over ResNet-20, distributed over ring topologies. Comp implies stochastic quantization [3] with 8 bits, which leads to $4 \times$ lower communication cost.

Agents	Comp	Method	CIFAR-10		CIFAR-100	
			$\alpha = 0.01$	$\alpha = 0.001$	$\alpha = 0.01$	$\alpha = 0.001$
5	✓	QGM	88.44 \pm 0.39	88.72 \pm 0.64	56.84 \pm 2.01	59.58 \pm 1.22
		QGM	86.85 \pm 0.73	86.82 \pm 0.99	48.80 \pm 8.58	51.99 \pm 4.23
	✓	<i>Q-SADDLe (ours)</i>	90.66 \pm 0.08	90.56 \pm 0.33	61.96 \pm 1.00	61.64 \pm 0.70
		<i>Q-SADDLe (ours)</i>	89.70 \pm 0.15	90.02 \pm 0.08	60.11 \pm 0.99	60.53 \pm 0.25
10	✓	QGM	77.41 \pm 8.00	79.48 \pm 2.76	48.06 \pm 4.36	44.16 \pm 6.71
		QGM	76.59 \pm 5.95	73.03 \pm 4.63	46.14 \pm 6.88	43.00 \pm 6.55
	✓	<i>Q-SADDLe (ours)</i>	87.72 \pm 1.59	86.33 \pm 0.24	58.06 \pm 0.68	56.76 \pm 0.86
		<i>Q-SADDLe (ours)</i>	87.82 \pm 1.42	85.57 \pm 1.33	57.90 \pm 0.82	56.27 \pm 0.84
20	✓	QGM	72.20 \pm 0.77	62.48 \pm 8.56	45.23 \pm 3.26	44.48 \pm 4.53
		QGM	66.61 \pm 6.68	60.30 \pm 6.60	43.64 \pm 3.68	42.75 \pm 1.82
	✓	<i>Q-SADDLe (ours)</i>	78.41 \pm 2.13	82.81 \pm 0.89	52.59 \pm 0.48	48.20 \pm 0.93
		<i>Q-SADDLe (ours)</i>	80.80 \pm 2.20	82.18 \pm 0.56	52.64 \pm 1.09	48.00 \pm 0.85
40	✓	QGM	70.46 \pm 4.14	60.86 \pm 0.98	40.15 \pm 0.90	38.73 \pm 1.47
		QGM	67.81 \pm 2.62	57.01 \pm 1.88	35.36 \pm 1.50	36.04 \pm 1.31
	✓	<i>Q-SADDLe (ours)</i>	77.49 \pm 0.83	73.54 \pm 2.04	43.25 \pm 1.71	41.99 \pm 1.27
		<i>Q-SADDLe (ours)</i>	76.35 \pm 0.42	72.03 \pm 2.12	41.75 \pm 2.14	41.03 \pm 0.67

Table 3 and 4 demonstrate the significant improvements in test accuracy and communication efficiency achieved by N-SADDLe over NGM[2]. As shown in Table 3, N-SADDLe outperforms NGM by 2.3% and 4.2% on average for CIFAR-10 and CIFAR-100, respectively. For CIFAR-10, the accuracy drop due to compression for NGM is $\sim 1-8\%$, while it is only about 0-0.3% for N-SADDLe. Similarly, for CIFAR-100, the drop due to compression for NGM is $\sim 2-11\%$, whereas for N-SADDLe, it is only 0-1.7%. These performance trends are maintained for ImageNette in Table 4, where N-SADDLe outperforms NGM by 1.7%, with a minimal drop of 1.4% with compression (as compared to 3.7% drop in case of NGM). To demonstrate the scalability of our approach, we present additional results on ImageNet distributed over a ring topology of 10 agents with varying degrees of heterogeneity. Our results in Table 4 show that N-SADDLe outperforms NGM by 4.2% while also being much

Table 2: Test accuracy of QGM, Q-SADDLe, and their compressed versions evaluated on Imagenette, distributed over a ring topology. Comp implies stochastic quantization [3] with 10-bits.

Agents	Comp	Method	Imagenette (MobileNet-V2)	
			$\alpha = 0.01$	$\alpha = 0.001$
5	✓	QGM	64.25 ± 11.53	57.67 ± 6.32
		QGM	59.86 ± 17.05	50.14 ± 9.39
	✓	<i>Q-SADDLe (ours)</i>	73.34 ± 0.80	72.50 ± 0.21
		<i>Q-SADDLe (ours)</i>	72.64 ± 1.66	72.77 ± 0.43
10	✓	QGM	56.30 ± 4.03	45.82 ± 5.99
		QGM	53.50 ± 5.66	36.71 ± 3.65
	✓	<i>Q-SADDLe (ours)</i>	62.35 ± 3.64	63.18 ± 1.59
		<i>Q-SADDLe (ours)</i>	63.35 ± 2.61	61.14 ± 0.71

Table 3: Test accuracy of NGM, N-SADDLe, and their compressed versions evaluated on CIFAR-10 and CIFAR-100 over ResNet-20, distributed with different degrees of heterogeneity over ring topologies. Comp implies 1-bit Sign SGD [24] based compression, which reduces the communication cost of the second round by 32× and the total communication cost by 1.94×.

Agents	Comp	Method	CIFAR-10		CIFAR-100	
			$\alpha = 0.01$	$\alpha = 0.001$	$\alpha = 0.01$	$\alpha = 0.001$
5	✓	NGM	90.87 ± 0.39	90.73 ± 0.46	59.00 ± 4.26	54.78 ± 4.68
		NGM	89.50 ± 0.68	87.69 ± 1.98	56.91 ± 1.82	50.65 ± 2.67
	✓	<i>N-SADDLe (ours)</i>	91.96 ± 0.19	91.69 ± 0.15	63.87 ± 0.45	64.10 ± 0.48
		<i>N-SADDLe (ours)</i>	91.88 ± 0.36	91.77 ± 0.19	62.35 ± 0.87	62.43 ± 0.36
10	✓	NGM	85.08 ± 2.73	83.43 ± 0.95	55.2 ± 1.41	54.70 ± 1.36
		NGM	76.85 ± 15.10	76.67 ± 3.67	43.41 ± 4.50	43.17 ± 4.65
	✓	<i>N-SADDLe (ours)</i>	88.43 ± 1.38	87.29 ± 1.23	59.31 ± 0.61	58.37 ± 0.30
		<i>N-SADDLe (ours)</i>	88.11 ± 1.54	87.14 ± 1.45	58.39 ± 0.89	58.33 ± 0.45
20	✓	NGM	84.84 ± 0.43	83.58 ± 0.89	53.98 ± 0.31	53.37 ± 0.53
		NGM	83.91 ± 0.96	78.90 ± 0.11	50.07 ± 2.79	46.73 ± 4.35
	✓	<i>N-SADDLe (ours)</i>	86.26 ± 0.29	86.61 ± 0.20	55.77 ± 0.53	55.14 ± 0.49
		<i>N-SADDLe (ours)</i>	86.34 ± 0.24	87.41 ± 0.52	56.65 ± 0.17	55.11 ± 1.16

Table 4: Test accuracy of NGM, N-SADDLe, and their compressed versions evaluated on ImageNette and ImageNet, distributed over a ring topology. Comp implies 1-bit Sign SGD based compression.

Agents	Comp	Method	Imagenette (MobileNet-V2)		ImageNet (ResNet-18)	
			$\alpha = 0.01$	$\alpha = 0.001$	$\alpha = 0.01$	$\alpha = 0.001$
10	✓	NGM	67.68 ± 1.23	67.10 ± 0.71	49.30	46.38
		NGM	63.65 ± 2.70	63.70 ± 0.87	34.66	34.40
	✓	<i>N-SADDLe (ours)</i>	69.54 ± 0.33	68.70 ± 0.79	52.20	51.94
		<i>N-SADDLe (ours)</i>	68.09 ± 0.57	67.37 ± 0.68	51.44	49.61

more robust to communication compression. Specifically, NGM incurs a significant drop of 13% in accuracy, compared to about a 1.5% drop for N-SADDLe.

We also evaluate our techniques on torus graph topology, and the results are presented in Table 7. Additionally, please refer to Table 8 in the Appendix for results on stochastic quantization-based compression for NGM and N-SADDLe. For the exact communication cost of all our presented experiments, please refer to Appendix C.7.

Impact of Varying Compression Levels: To understand the impact of the degree of compression, we evaluate QGM, Q-SADDLe, NGM, and N-SADDLe for a range of quantization levels and present the results in Figure 3. Test accuracy for QGM drops from about 79% to 73% as the compression becomes more extreme, while Q-SADDLe retains its performance with a minimal drop of $\sim 0.7\%$. Similarly, NGM incurs an accuracy drop of about $\sim 7\%$ due to compression, while N-SADDLe maintains its performance.

Evaluating Flatness Measures: To confirm our hypothesis that the presence of SAM in decentralized training leads to a flatter loss landscape, we compute the highest eigenvalue λ_{\max} of the Hessian at different epochs during the training [15]. Note that lower the λ_{\max} , flatter the loss landscape [21, 14, 12]. As shown in Figure 4, Q-SADDLe and Comp Q-SADDLe have consistently lower λ_{\max} as compared to QGM and Comp QGM, respectively. This enhances the robustness of Q-SADDLe

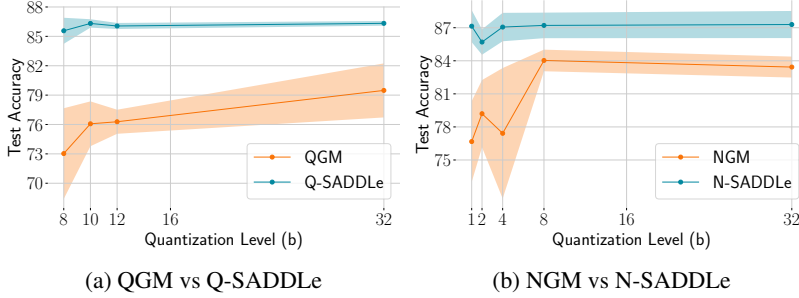


Figure 3: Test accuracy for different levels of quantization-based compression scheme for CIFAR-10 over a 10 agent ring topology. Note that $b = 32$ represents the full communication baseline.

to erroneous updates due to communication compression. The difference in the eigenvalues is remarkably high towards the end of the training, indicating that models trained with SAM converge to a flatter minimum as expected. Please refer to Figure 6 and 7 in the Appendix for loss landscape visualization.

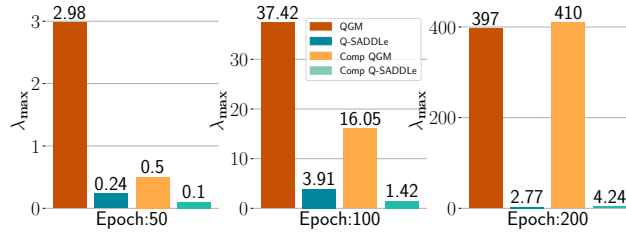


Figure 4: Largest Eigenvalue of the Hessian (λ_{\max}) at 3 different stages of training for ResNet-20 trained on CIFAR-10 in a 10 agent ring topology with $\alpha = 0.001$.

7 Limitations and Future Work

This section discusses two potential limitations of our proposed approach: 1) SADDLe assumes the mixing matrix \mathbf{W} to be doubly stochastic and symmetric, making it incompatible with time-varying and directed graphs. To address this, SADDLe can be combined with Stochastic Gradient Push (SGP) [6]. 2) SADDLe utilizes SAM to seek flatter loss landscapes and hence requires an additional backward pass to compute the perturbation ξ_i as shown in equation 3. One potential way to reduce the computational cost of our approach is to employ the recently proposed compute-efficient variants of SAM [12, 36, 37]. As a future research direction, the theoretical analysis for SADDLe presented in Section 5 can be extended to settings where communication compression is employed. Moreover, it has been shown that communication compression only affects the higher order terms in the convergence rate [26, 45].

8 Conclusion

Communication-efficient decentralized learning on heterogeneous data is crucial for enabling on-device learning to leverage huge amounts of user-generated data. In this work, we propose Sharpness-Aware Decentralized Deep Learning (SADDLe) to improve generalization and communication efficiency in the presence of data heterogeneity. SADDLe aims to seek a flatter loss landscape during training through gradient perturbation via SAM[14]. Our theoretical analysis shows that SADDLe achieves a convergence rate that is on par with well-known decentralized convergence bounds [33]. SADDLe is orthogonal to existing decentralized learning algorithms and can be used in synergy to boost performance. To that effect, we present two versions of our approach, Q-SADDLe and N-SADDLe, and conduct an exhaustive set of experiments to evaluate these techniques over various datasets, models, graphs, and compression schemes. Our results show that SADDLe leads to 1-20% better accuracy than existing decentralized algorithms for non-IID data, with a minimal drop of $\sim 1\%$ on average in the presence of up to $4\times$ communication compression.

Acknowledgements

This work was supported by the Center for the Co-Design of Cognitive Systems (COCOSYS), a DARPA-sponsored JUMP center, the Semiconductor Research Corporation (SRC), and the National Science Foundation.

References

- [1] S. A. Aketi, A. Hashemi, and K. Roy. Global update tracking: A decentralized learning algorithm for heterogeneous data. In A. Oh, T. Neumann, A. Globerson, K. Saenko, M. Hardt, and S. Levine, editors, *Advances in Neural Information Processing Systems*, volume 36, pages 48939–48961. Curran Associates, Inc., 2023. URL https://proceedings.neurips.cc/paper_files/paper/2023/file/98f8c89ae042c512e6c87e0e0c2a0f98-Paper-Conference.pdf.
- [2] S. A. Aketi, S. Kodge, and K. Roy. Neighborhood gradient mean: An efficient decentralized learning method for non-IID data. *Transactions on Machine Learning Research*, 2023. ISSN 2835-8856. URL <https://openreview.net/forum?id=vkiKzK5G3e>.
- [3] D. Alistarh, D. Grubic, J. Li, R. Tomioka, and M. Vojnovic. Qsgd: Communication-efficient sgd via gradient quantization and encoding. In I. Guyon, U. V. Luxburg, S. Bengio, H. Wallach, R. Fergus, S. Vishwanathan, and R. Garnett, editors, *Advances in Neural Information Processing Systems*, volume 30. Curran Associates, Inc., 2017. URL https://proceedings.neurips.cc/paper_files/paper/2017/file/6c340f25839e6acdc73414517203f5f0-Paper.pdf.
- [4] D. Alistarh, T. Hoefler, M. Johansson, N. Konstantinov, S. Khirirat, and C. Renggli. The convergence of sparsified gradient methods. In S. Bengio, H. Wallach, H. Larochelle, K. Grauman, N. Cesa-Bianchi, and R. Garnett, editors, *Advances in Neural Information Processing Systems*, volume 31. Curran Associates, Inc., 2018. URL https://proceedings.neurips.cc/paper_files/paper/2018/file/314450613369e0ee72d0da7f6fee773c-Paper.pdf.
- [5] M. Andriushchenko and N. Flammarion. Towards understanding sharpness-aware minimization. In *International Conference on Machine Learning*, pages 639–668. PMLR, 2022.
- [6] M. Assran, N. Loizou, N. Ballas, and M. Rabbat. Stochastic gradient push for distributed deep learning. In *International Conference on Machine Learning*, pages 344–353. PMLR, 2019.
- [7] A. Balu, Z. Jiang, S. Y. Tan, C. Hedge, Y. M. Lee, and S. Sarkar. Decentralized deep learning using momentum-accelerated consensus. In *ICASSP 2021 - 2021 IEEE International Conference on Acoustics, Speech and Signal Processing (ICASSP)*, pages 3675–3679, 2021. doi: 10.1109/ICASSP39728.2021.9414564.
- [8] D. Caldarola, B. Caputo, and M. Ciccone. Improving generalization in federated learning by seeking flat minima. In *European Conference on Computer Vision*, pages 654–672. Springer, 2022.
- [9] R. Dai, X. Yang, Y. Sun, L. Shen, X. Tian, M. Wang, and Y. Zhang. Fedgamma: Federated learning with global sharpness-aware minimization. *IEEE Transactions on Neural Networks and Learning Systems*, pages 1–14, 2023. doi: 10.1109/TNNLS.2023.3304453.
- [10] J. Dean, G. Corrado, R. Monga, K. Chen, M. Devin, M. Mao, M. Ranzato, A. Senior, P. Tucker, K. Yang, et al. Large scale distributed deep networks. *Advances in neural information processing systems*, 25, 2012.
- [11] J. Deng, W. Dong, R. Socher, L.-J. Li, K. Li, and L. Fei-Fei. Imagenet: A large-scale hierarchical image database. In *2009 IEEE conference on computer vision and pattern recognition*, pages 248–255. Ieee, 2009.
- [12] J. Du, Z. Daquan, J. Feng, V. Tan, and J. T. Zhou. Sharpness-aware training for free. In A. H. Oh, A. Agarwal, D. Belgrave, and K. Cho, editors, *Advances in Neural Information Processing Systems*, 2022. URL <https://openreview.net/forum?id=xK6wRfL2mv7>.
- [13] Y. Esfandiari, S. Y. Tan, Z. Jiang, A. Balu, E. Herron, C. Hegde, and S. Sarkar. Cross-gradient aggregation for decentralized learning from non-iid data. In *International Conference on Machine Learning*, pages 3036–3046. PMLR, 2021.

- [14] P. Foret, A. Kleiner, H. Mobahi, and B. Neyshabur. Sharpness-aware minimization for efficiently improving generalization. In *International Conference on Learning Representations*, 2021. URL <https://openreview.net/forum?id=6Tm1mposlrM>.
- [15] N. Golmant, A. Gholami, M. Mahoney, and J. Gonzalez. pytorch-hessian-eigenthings: efficient pytorch hessian eigendecomposition, Oct. 2018. URL <https://github.com/noahgolmant/pytorch-hessian-eigenthings>.
- [16] K. He, X. Zhang, S. Ren, and J. Sun. Deep residual learning for image recognition. In *Proceedings of the IEEE conference on computer vision and pattern recognition*, pages 770–778, 2016.
- [17] K. Hsieh, A. Phanishayee, O. Mutlu, and P. B. Gibbons. The non-iid data quagmire of decentralized machine learning. In *Proceedings of the 37th International Conference on Machine Learning*, ICML’20. JMLR.org, 2020.
- [18] K. Hsieh, A. Phanishayee, O. Mutlu, and P. B. Gibbons. The non-iid data quagmire of decentralized machine learning. In *Proceedings of the 37th International Conference on Machine Learning*, ICML’20. JMLR.org, 2020.
- [19] T.-M. H. Hsu, H. Qi, and M. Brown. Measuring the effects of non-identical data distribution for federated visual classification. *arXiv preprint arXiv:1909.06335*, 2019.
- [20] H. Husain. Imagenette - a subset of 10 easily classified classes from the imagenet dataset. <https://github.com/fastai/imagenette>, 2018.
- [21] S. Jastrzebski, M. Szymczak, S. Fort, D. Arpit, J. Tabor, K. Cho, and K. Geras. The break-even point on optimization trajectories of deep neural networks. *arXiv preprint arXiv:2002.09572*, 2020.
- [22] W. Jiang, H. Yang, Y. Zhang, and J. Kwok. An adaptive policy to employ sharpness-aware minimization. *arXiv preprint arXiv:2304.14647*, 2023.
- [23] Y. Jiang*, B. Neyshabur*, H. Mobahi, D. Krishnan, and S. Bengio. Fantastic generalization measures and where to find them. In *International Conference on Learning Representations*, 2020. URL <https://openreview.net/forum?id=SJgIPJBFvH>.
- [24] S. P. Karimireddy, Q. Rebjock, S. Stich, and M. Jaggi. Error feedback fixes signsgd and other gradient compression schemes. In *International Conference on Machine Learning*, pages 3252–3261. PMLR, 2019.
- [25] N. S. Keskar, D. Mudigere, J. Nocedal, M. Smelyanskiy, and P. T. P. Tang. On large-batch training for deep learning: Generalization gap and sharp minima. In *International Conference on Learning Representations*, 2017. URL <https://openreview.net/forum?id=H1oyRlYgg>.
- [26] A. Koloskova, T. Lin, S. U. Stich, and M. Jaggi. Decentralized deep learning with arbitrary communication compression. *arXiv preprint arXiv:1907.09356*, 2019.
- [27] A. Koloskova, S. Stich, and M. Jaggi. Decentralized stochastic optimization and gossip algorithms with compressed communication. In K. Chaudhuri and R. Salakhutdinov, editors, *Proceedings of the 36th International Conference on Machine Learning*, volume 97 of *Proceedings of Machine Learning Research*, pages 3478–3487. PMLR, 09–15 Jun 2019. URL <https://proceedings.mlr.press/v97/koloskova19a.html>.
- [28] A. Koloskova, T. Lin, and S. U. Stich. An improved analysis of gradient tracking for decentralized machine learning. *Advances in Neural Information Processing Systems*, 34:11422–11435, 2021.
- [29] J. Konečný, H. B. McMahan, D. Ramage, and P. Richtárik. Federated optimization: Distributed machine learning for on-device intelligence. 2016.
- [30] A. Krizhevsky, V. Nair, and G. Hinton. Cifar (canadian institute for advanced research). <http://www.cs.toronto.edu/kriz/cifar.html>, 2014.
- [31] J. Kwon, J. Kim, H. Park, and I. K. Choi. Asam: Adaptive sharpness-aware minimization for scale-invariant learning of deep neural networks. In *Proceedings of the 38th International Conference on Machine Learning*, Proceedings of Machine Learning Research, pages 5905–5914. PMLR, 2021. URL <https://proceedings.mlr.press/v139/kwon21b.html>.

- [32] H. Li, Z. Xu, G. Taylor, C. Studer, and T. Goldstein. Visualizing the loss landscape of neural nets. In S. Bengio, H. Wallach, H. Larochelle, K. Grauman, N. Cesa-Bianchi, and R. Garnett, editors, *Advances in Neural Information Processing Systems*, volume 31. Curran Associates, Inc., 2018. URL https://proceedings.neurips.cc/paper_files/paper/2018/file/a41b3bb3e6b050b6c9067c67f663b915-Paper.pdf.
- [33] X. Lian, C. Zhang, H. Zhang, C.-J. Hsieh, W. Zhang, and J. Liu. Can decentralized algorithms outperform centralized algorithms? a case study for decentralized parallel stochastic gradient descent. *Advances in Neural Information Processing Systems*, 30, 2017.
- [34] T. Lin, S. P. Karimireddy, S. Stich, and M. Jaggi. Quasi-global momentum: Accelerating decentralized deep learning on heterogeneous data. In *Proceedings of the 38th International Conference on Machine Learning*, volume 139 of *Proceedings of Machine Learning Research*, pages 6654–6665. PMLR, 18–24 Jul 2021.
- [35] H. Liu, A. Brock, K. Simonyan, and Q. Le. Evolving normalization-activation layers. In H. Larochelle, M. Ranzato, R. Hadsell, M. Balcan, and H. Lin, editors, *Advances in Neural Information Processing Systems*, volume 33, pages 13539–13550. Curran Associates, Inc., 2020. URL https://proceedings.neurips.cc/paper_files/paper/2020/file/9d4c03631b8b0c85ae08bf05eda37d0f-Paper.pdf.
- [36] Y. Liu, S. Mai, X. Chen, C.-J. Hsieh, and Y. You. Towards efficient and scalable sharpness-aware minimization. In *Proceedings of the IEEE/CVF Conference on Computer Vision and Pattern Recognition*, pages 12360–12370, 2022.
- [37] P. Mi, L. Shen, T. Ren, Y. Zhou, X. Sun, R. Ji, and D. Tao. Make sharpness-aware minimization stronger: A sparsified perturbation approach. In A. H. Oh, A. Agarwal, D. Belgrave, and K. Cho, editors, *Advances in Neural Information Processing Systems*, 2022. URL https://openreview.net/forum?id=88_wNI6ZBDZ.
- [38] Z. Qu, X. Li, R. Duan, Y. Liu, B. Tang, and Z. Lu. Generalized federated learning via sharpness aware minimization. In *International conference on machine learning*, pages 18250–18280. PMLR, 2022.
- [39] M. Sandler, A. Howard, M. Zhu, A. Zhmoginov, and L.-C. Chen. Mobilenetv2: Inverted residuals and linear bottlenecks. In *Proceedings of the IEEE conference on computer vision and pattern recognition*, pages 4510–4520, 2018.
- [40] Y. Shi, L. Shen, K. Wei, Y. Sun, B. Yuan, X. Wang, and D. Tao. Improving the model consistency of decentralized federated learning. In *International Conference on Machine Learning*, pages 31269–31291. PMLR, 2023.
- [41] S. U. Stich, J.-B. Cordonnier, and M. Jaggi. Sparsified sgd with memory. NIPS’18, page 4452–4463, Red Hook, NY, USA, 2018. Curran Associates Inc.
- [42] Y. Sun, L. Shen, S. Chen, L. Ding, and D. Tao. Dynamic regularized sharpness aware minimization in federated learning: Approaching global consistency and smooth landscape. In *International Conference on Machine Learning*, pages 32991–33013. PMLR, 2023.
- [43] H. Tang, S. Gan, C. Zhang, T. Zhang, and J. Liu. Communication compression for decentralized training. In *Proceedings of the 32nd International Conference on Neural Information Processing Systems*, NIPS’18, page 7663–7673, Red Hook, NY, USA, 2018. Curran Associates Inc.
- [44] H. Tang, X. Lian, M. Yan, C. Zhang, and J. Liu. d^2 : Decentralized training over decentralized data. In J. Dy and A. Krause, editors, *Proceedings of the 35th International Conference on Machine Learning*, volume 80 of *Proceedings of Machine Learning Research*, pages 4848–4856. PMLR, 10–15 Jul 2018. URL <https://proceedings.mlr.press/v80/tang18a.html>.
- [45] H. Tang, X. Lian, S. Qiu, L. Yuan, C. Zhang, T. Zhang, and J. Liu. Deepsqueeze: Decentralization meets error-compensated compression. *arXiv preprint arXiv:1907.07346*, 2019.
- [46] T. Vogels, S. P. Karimireddy, and M. Jaggi. Practical low-rank communication compression in decentralized deep learning. In H. Larochelle, M. Ranzato, R. Hadsell, M. Balcan, and H. Lin, editors, *Advances in Neural Information Processing Systems*, volume 33, pages 14171–14181. Curran Associates, Inc., 2020. URL https://proceedings.neurips.cc/paper_files/paper/2020/file/a376802c0811f1b9088828288eb0d3f0-Paper.pdf.
- [47] L. Xiao and S. Boyd. Fast linear iterations for distributed averaging. *Systems & Control Letters*, 53(1):65–78, 2004.

- [48] H. Zhao, B. Li, Z. Li, P. Richtárik, and Y. Chi. BEER: Fast $\mathcal{O}(1/t)$ rate for decentralized nonconvex optimization with communication compression. In A. H. Oh, A. Agarwal, D. Belgrave, and K. Cho, editors, *Advances in Neural Information Processing Systems*, 2022. URL <https://openreview.net/forum?id=I47eFCka1f3>.
- [49] Y. Zhao, H. Zhang, and X. Hu. Penalizing gradient norm for efficiently improving generalization in deep learning. In *International Conference on Machine Learning*, pages 26982–26992. PMLR, 2022.

A Theoretical Analysis

The update rule for Q-SADDLe with SAM-based gradient $\tilde{\mathbf{G}}$ is as follows:

$$\begin{aligned}\mathbf{X}^{(t+1)} &= \mathbf{W} \left(\mathbf{X}^{(t)} - \eta \left(\beta \mathbf{M}^{(t)} + \tilde{\mathbf{G}}^{(t)} \right) \right) \\ \mathbf{M}^{(t+1)} &= \mu \mathbf{M}^{(t)} + (1 - \mu) \frac{\mathbf{X}^{(t)} - \mathbf{X}^{(t+1)}}{\eta} \\ &= (\mu + (1 - \mu)\beta \mathbf{W}) \mathbf{M}^{(t)} + (1 - \mu) \mathbf{W} \tilde{\mathbf{G}}^{(t)} + \frac{1 - \mu}{\eta} (\mathbf{I} - \mathbf{W}) \mathbf{X}^{(t)},\end{aligned}\tag{8}$$

For a doubly stochastic mixing matrix \mathbf{W} , we can simplify the updates as follows:

$$\begin{aligned}\bar{\mathbf{x}}^{(t+1)} &= \bar{\mathbf{x}}^{(t)} - \eta \left(\beta \bar{\mathbf{m}}^{(t)} + \frac{1}{n} \sum_{i=1}^n \tilde{\mathbf{g}}_i^t \right), \\ \bar{\mathbf{m}}^{(t+1)} &= \mu \bar{\mathbf{m}}^{(t)} + (1 - \mu) \frac{\bar{\mathbf{x}}^{(t)} - \bar{\mathbf{x}}^{(t+1)}}{\eta} = (1 - (1 - \mu)(1 - \beta)) \bar{\mathbf{m}}^{(t)} + (1 - \mu) \frac{1}{n} \sum_{i=1}^n \tilde{\mathbf{g}}_i^t.\end{aligned}\tag{9}$$

Here, $\tilde{\mathbf{g}}_i^t$ is the SAM-based gradient update, which we reiterate for ease of understanding :

$$\tilde{\mathbf{g}}_i^t = \nabla F_i(\mathbf{x}_i^t + \xi(\mathbf{x}_i^t); d_i^t), \quad \text{where } \xi(\mathbf{x}_i^t) = \rho \frac{\mathbf{g}_i^t}{\|\mathbf{g}_i^t\|}\tag{10}$$

For the rest of the analysis, we use $\xi(\mathbf{x}_i^t) = \xi_i^t$ for simplicity of notation. We introduce the following lemma to define an upper bound on the stochastic variance of SAM-based updates.

Lemma 3 *Given assumptions 1-3, the stochastic variance of local gradients with perturbation can be bounded as*

$$\|\nabla F_i(\mathbf{x}_i + \xi_i) - \nabla f_i(\mathbf{x}_i + \xi_i)\|^2 \leq 3\sigma^2 + 6L^2\rho^2\tag{11}$$

Proof:

$$\begin{aligned}& \|\nabla F_i(\mathbf{x}_i + \xi_i) - \nabla f_i(\mathbf{x}_i + \xi_i)\|^2 = \\ & \|\nabla F_i(\mathbf{x}_i + \xi_i) - \nabla F_i(\mathbf{x}_i) + \nabla F_i(\mathbf{x}_i) - \nabla f_i(\mathbf{x}_i) + \nabla f_i(\mathbf{x}_i) - \nabla f_i(\mathbf{x}_i + \xi_i)\|^2 \\ & \stackrel{a}{\leq} 3\|\nabla F_i(\mathbf{x}_i + \xi_i) - \nabla F_i(\mathbf{x}_i)\|^2 + 3\|\nabla F_i(\mathbf{x}_i) - \nabla f_i(\mathbf{x}_i)\|^2 + 3\|\nabla f_i(\mathbf{x}_i) - \nabla f_i(\mathbf{x}_i + \xi_i)\|^2 \\ & \stackrel{b}{\leq} 3\|\nabla F_i(\mathbf{x}_i + \xi_i) - \nabla F_i(\mathbf{x}_i)\|^2 + 3\sigma^2 + 3\|\nabla f_i(\mathbf{x}_i) - \nabla f_i(\mathbf{x}_i + \xi_i)\|^2 \stackrel{c}{\leq} 3\sigma^2 + 6L^2\rho^2\end{aligned}\tag{12}$$

(a) follows from the property $\|x_1 + x_2 + \dots + x_n\|^2 \leq n[\|x_1\|^2 + \|x_2\|^2 + \dots + \|x_n\|^2]$ for random variables x_1, x_2, \dots, x_n . (b) follows from equation 5 in Assumption 2. (c) follows from Assumption 1 and the perturbation ξ_i being bounded by the perturbation radius ρ .

Lemma 4 *Given assumptions 1-3 and $\tilde{\mathbf{g}}_i = \nabla F_i(\mathbf{x}_i + \xi_i)$, the following relationship holds*

$$\mathbb{E}\left[\left\|\frac{1}{n} \sum_{i=1}^n \tilde{\mathbf{g}}_i\right\|^2\right] \leq \frac{3\sigma^2}{n} + \frac{6L^2\rho^2}{n} + \mathbb{E}\left[\left\|\frac{1}{n} \sum_{i=1}^n \nabla f_i(\mathbf{x}_i + \xi_i)\right\|^2\right]\tag{13}$$

Proof:

$$\begin{aligned}\mathbb{E}\left[\left\|\frac{1}{n} \sum_{i=1}^n \tilde{\mathbf{g}}_i\right\|^2\right] &= \mathbb{E}\left[\left\|\frac{1}{n} \sum_{i=1}^n \tilde{\mathbf{g}}_i - \nabla f_i(\mathbf{x}_i + \xi_i)\right\|^2\right] + \mathbb{E}\left[\left\|\frac{1}{n} \sum_{i=1}^n \nabla f_i(\mathbf{x}_i + \xi_i)\right\|^2\right] \\ &= \frac{1}{n^2} \mathbb{E}\left[\sum_{i=1}^n \|\tilde{\mathbf{g}}_i - \nabla f_i(\mathbf{x}_i + \xi_i)\|^2\right] + \mathbb{E}\left[\left\|\frac{1}{n} \sum_{i=1}^n \nabla f_i(\mathbf{x}_i + \xi_i)\right\|^2\right] \\ &\leq \frac{3\sigma^2}{n} + \frac{6L^2\rho^2}{n} + \mathbb{E}\left[\left\|\frac{1}{n} \sum_{i=1}^n \nabla f_i(\mathbf{x}_i + \xi_i)\right\|^2\right]\end{aligned}\tag{14}$$

As a first step, we simplify our convergence analysis by defining another sequence of parameters $\mathbf{z}^{(t)}$ with the following update rule:

$$\mathbf{z}^{(t+1)} = \mathbf{z}^{(t)} - \left(\frac{\eta}{1-\beta} \right) \frac{1}{n} \sum_{i=1}^n \tilde{\mathbf{g}}_i^t \quad (15)$$

Inspired by QGM [34], this sequence has a simpler SAM update rule, while our parameters $\bar{\mathbf{x}}^{(t)}$ follow SAM based gradient updates along with a momentum buffer \mathbf{m}_i^t . We use $\bar{\mathbf{g}}^{(t)} = \frac{1}{n} \sum_{i=1}^n \tilde{\mathbf{g}}_i^t$ and $\tilde{\eta} = \frac{\eta}{1-\beta}$ for rest of the analysis. We begin by proving that the error $\mathbf{e}^{(t)} = \mathbf{z}^{(t)} - \bar{\mathbf{x}}^{(t)}$ remains bounded.

Lemma 5 *Given Assumptions 1-3, the sequence of iterates generated by Q-SADDLe satisfy*

$$\mathbb{E} \left\| \mathbf{e}^{(t+1)} \right\|^2 \leq (1 - (1-\mu)(1-\beta)) \mathbb{E} \left\| \mathbf{e}^{(t)} \right\|^2 + \frac{2\tilde{\eta}^2 \beta^2}{(1-\beta)(1-\mu)} \mathbb{E} \left\| \frac{1}{n} \sum_{i=1}^n \nabla f_i(\mathbf{x}_i + \xi_i) \right\|^2 + 3\tilde{\eta}^2 \beta^2 \sigma^2 + 6\tilde{\eta}^2 \beta^2 L^2 \rho^2.$$

Proof: For $\mathbf{e}^{(0)} = 0$, specifying $\mathbf{e}^{(t+1)}$ in terms of update sequences $\mathbf{z}^{(t+1)}$ and $\bar{\mathbf{x}}^{(t+1)}$:

$$\begin{aligned} \mathbf{e}^{(t+1)} &= \mathbf{z}^{(t+1)} - \bar{\mathbf{x}}^{(t+1)} = \left(\mathbf{z}^{(t)} - \frac{\eta}{1-\beta} \bar{\mathbf{g}}^{(t)} \right) - \left(\bar{\mathbf{x}}^{(t)} - \eta(\beta \bar{\mathbf{m}}^{(t)} + \bar{\mathbf{g}}^{(t)}) \right) \\ &= \mathbf{e}^{(t)} - \eta\beta \left(\frac{1}{1-\beta} \bar{\mathbf{g}}^{(t)} - \bar{\mathbf{m}}^{(t)} \right) = \sum_{k=0}^t -\eta\beta \left(\frac{1}{1-\beta} \bar{\mathbf{g}}^{(k)} - \bar{\mathbf{m}}^{(k)} \right). \end{aligned} \quad (16)$$

Using equation (9), we have [34]:

$$\begin{aligned} \mathbf{e}^{(t+1)} &= \sum_{k=0}^{(t)} -\eta\beta \left(\frac{1}{1-\beta} \bar{\mathbf{g}}^{(k)} - \left((1 - (1-\mu)(1-\beta)) \bar{\mathbf{m}}^{(k-1)} + (1-\mu) \bar{\mathbf{g}}^{(k-1)} \right) \right) \\ &= (1 - (1-\mu)(1-\beta)) \sum_{k=0}^t -\eta\beta \left(\frac{1}{1-\beta} \bar{\mathbf{g}}^{(k-1)} - \bar{\mathbf{m}}^{(k-1)} \right) + \sum_{k=0}^{(t)} -\frac{\eta\beta}{1-\beta} \left(\bar{\mathbf{g}}^{(k)} - \bar{\mathbf{g}}^{(k-1)} \right) \\ &= (1 - (1-\mu)(1-\beta)) \mathbf{e}^{(t)} - \frac{\eta\beta}{1-\beta} \bar{\mathbf{g}}^{(t)}. \end{aligned} \quad (17)$$

Taking expectation of $\|\mathbf{e}^{(t+1)}\|^2$:

$$\begin{aligned} \mathbb{E} \left\| \mathbf{e}^{(t+1)} \right\|^2 &= \mathbb{E} \left\| (1 - (1-\mu)(1-\beta)) \mathbf{e}^{(t)} - \frac{\eta\beta}{1-\beta} \bar{\mathbf{g}}^{(t)} \right\|^2 \\ &\stackrel{a}{\leq} \mathbb{E} \left\| (1 - (1-\mu)(1-\beta)) \mathbf{e}^{(t)} - \frac{\eta\beta}{1-\beta} \mathbb{E}_t[\bar{\mathbf{g}}^{(t)}] \right\|^2 + \left(\frac{\eta^2 \beta^2}{(1-\beta)^2} \right) (3\sigma^2 + 6L^2 \rho^2) \\ &\leq (1 - (1-\mu)(1-\beta)) \mathbb{E} \left\| \mathbf{e}^{(t)} \right\|^2 + \frac{2\tilde{\eta}^2 \beta^2}{(1-\beta)(1-\mu)} \mathbb{E} \left\| \frac{1}{n} \sum_{i=1}^n \nabla f_i(\mathbf{x}_i + \xi_i) \right\|^2 \\ &\quad + 3\tilde{\eta}^2 \beta^2 \sigma^2 + 6\tilde{\eta}^2 \beta^2 L^2 \rho^2. \end{aligned} \quad (18)$$

(a) is the result of Lemma 3.

We now proceed to bound the consensus error.

Lemma 6 *Given Assumptions 1-3, the sequence of iterates generated by Q-SADDLe satisfy,*

$$\begin{aligned} \frac{1}{n} \mathbb{E} \left\| \mathbf{X}^{t+1} - \bar{\mathbf{X}}^{t+1} \right\|^2 &\leq \frac{(1-\lambda/4)}{n} \mathbb{E} \left\| \mathbf{X}^t - \bar{\mathbf{X}}^t \right\|^2 + \frac{24\eta^2 L^2 \rho^2}{\lambda} + \frac{12\eta^2 \delta^2}{\lambda} \\ &\quad + 12\eta^2 (1-\lambda) (\sigma^2 + 2L^2 \rho^2) + \frac{6\tilde{\eta}^2 \beta^2}{\lambda n} \mathbb{E} \left\| \mathbf{M}^{(t)} - \bar{\mathbf{M}}^{(t)} \right\|^2. \end{aligned} \quad (19)$$

Proof: We start by describing \mathbf{X}^{t+1} and $\bar{\mathbf{X}}^{t+1}$ in terms of the update rule in equation 8:

$$\begin{aligned}
& \frac{1}{n} \mathbb{E} \left\| \mathbf{X}^{t+1} - \bar{\mathbf{X}}^{t+1} \right\|^2 = \frac{1}{n} \mathbb{E} \left\| \mathbf{W} \left(\mathbf{X}^{(t)} - \eta \left(\beta \mathbf{M}^{(t)} + \tilde{\mathbf{G}}^{(t)} \right) \right) - \left(\bar{\mathbf{X}}^{(t)} - \eta \left(\beta \bar{\mathbf{M}}^{(t)} + \bar{\mathbf{G}}^{(t)} \right) \right) \right\|^2 \\
& \stackrel{a}{\leq} \frac{1-\lambda}{n} \mathbb{E} \left\| \left(\mathbf{X}^{(t)} - \eta \left(\beta \mathbf{M}^{(t)} + \tilde{\mathbf{G}}^{(t)} \right) \right) - \left(\bar{\mathbf{X}}^{(t)} - \eta \left(\beta \bar{\mathbf{M}}^{(t)} + \bar{\mathbf{G}}^{(t)} \right) \right) \right\|^2 \\
& \stackrel{b}{\leq} \frac{1-\lambda}{n} \mathbb{E} \left\| \left(\mathbf{X}^{(t)} - \eta \left(\beta \mathbf{M}^{(t)} + \mathbb{E}_t \left[\tilde{\mathbf{G}}^{(t)} \right] \right) \right) - \left(\bar{\mathbf{X}}^{(t)} - \eta \left(\beta \bar{\mathbf{M}}^{(t)} + \mathbb{E}_t \left[\bar{\mathbf{G}}^{(t)} \right] \right) \right) \right\|^2 \\
& \quad + 12\eta^2(1-\lambda)(\sigma^2 + 2L^2\rho^2) \\
& \leq \frac{(1-\lambda)(1+\lambda/2)}{n} \mathbb{E} \left\| \mathbf{X}^{(t)} - \bar{\mathbf{X}}^{(t)} \right\|^2 + \frac{6\eta^2\beta^2}{\lambda n} \mathbb{E} \left\| \mathbf{M}^{(t)} - \bar{\mathbf{M}}^{(t)} \right\|^2 \\
& \quad + \frac{6\eta^2}{\lambda n} \underbrace{\mathbb{E} \left\| \mathbb{E}_t \left[\tilde{\mathbf{G}}^{(t)} \right] - \mathbb{E}_t \left[\bar{\mathbf{G}}^{(t)} \right] \right\|^2}_{\star} + 12\eta^2(1-\lambda)(\sigma^2 + 2L^2\rho^2).
\end{aligned} \tag{20}$$

(a) comes from Assumption 3 on Mixing matrix. (b) results from $\tilde{\mathbf{G}}^{(t)} = \mathbb{E}_t \left[\tilde{\mathbf{G}}^{(t)} \right] + \tilde{\mathbf{G}}^{(t)} - \mathbb{E}_t \left[\tilde{\mathbf{G}}^{(t)} \right]$ and Lemma 3.

We first analyze \star :

$$\begin{aligned}
& \mathbb{E} \left\| \mathbb{E}_t \left[\tilde{\mathbf{G}}^{(t)} \right] - \mathbb{E}_t \left[\bar{\mathbf{G}}^{(t)} \right] \right\|^2 = \sum_{i=1}^n \mathbb{E} \left\| \nabla f_i(\mathbf{x}_i^{(t)} + \xi_i^{(t)}) \pm \nabla f_i(\bar{\mathbf{x}}^{(t)}) - \nabla f(\bar{\mathbf{x}}^{(t)}) \right\|^2 \\
& \leq 2 \sum_{i=1}^n \mathbb{E} \left\| \nabla f_i(\mathbf{x}_i^{(t)} + \xi_i^{(t)}) - \nabla f_i(\bar{\mathbf{x}}^{(t)}) \right\|^2 + 2 \sum_{i=1}^n \mathbb{E} \left\| \nabla f_i(\bar{\mathbf{x}}^{(t)}) - \nabla f(\bar{\mathbf{x}}^{(t)}) \right\|^2 \\
& \stackrel{a}{\leq} 2L^2 \sum_{i=1}^n \mathbb{E} \left\| \mathbf{x}_i^{(t)} + \xi_i^{(t)} - \bar{\mathbf{x}}^{(t)} \right\|^2 + 2n\delta^2 \\
& \stackrel{b}{\leq} 4L^2 \sum_{i=1}^n \mathbb{E} \left\| \mathbf{x}_i^{(t)} - \bar{\mathbf{x}}^{(t)} \right\|^2 + 4nL^2\rho^2 + 2n\delta^2
\end{aligned} \tag{21}$$

(a) follows from Assumption 1, and (b) is the result of perturbation being bounded by the perturbation radius ρ .

Substituting the result of equation 21 in 20:

$$\begin{aligned}
& \frac{1}{n} \mathbb{E} \left\| \mathbf{X}^{t+1} - \bar{\mathbf{X}}^{t+1} \right\|^2 \leq \frac{(1-\lambda/2)}{n} \mathbb{E} \left\| \mathbf{X}^{(t)} - \bar{\mathbf{X}}^{(t)} \right\|^2 + \frac{6\eta^2\beta^2}{\lambda n} \mathbb{E} \left\| \mathbf{M}^{(t)} - \bar{\mathbf{M}}^{(t)} \right\|^2 \\
& \quad + \frac{24\eta^2L^2}{\lambda n} \left(\sum_{i=1}^n \mathbb{E} \left\| \mathbf{x}_i^{(t)} - \bar{\mathbf{x}}^{(t)} \right\|^2 \right) + \frac{24\eta^2L^2\rho^2}{\lambda} + \frac{12\eta^2\delta^2}{\lambda} \\
& \quad + 12\eta^2(1-\lambda)(\sigma^2 + 2L^2\rho^2)
\end{aligned} \tag{22}$$

The assumption that learning rate $\eta \leq \frac{\lambda}{10L}$ ensures that $24\eta^2L^2 \leq \lambda^2/4$. Modifying the above equation through this and rearranging the terms we have:

$$\begin{aligned}
& \frac{1}{n} \mathbb{E} \left\| \mathbf{X}^{t+1} - \bar{\mathbf{X}}^{t+1} \right\|^2 \leq \frac{(1-\lambda/4)}{n} \mathbb{E} \left\| \mathbf{X}^{(t)} - \bar{\mathbf{X}}^{(t)} \right\|^2 + \frac{6\eta^2\beta^2}{\lambda n} \mathbb{E} \left\| \mathbf{M}^{(t)} - \bar{\mathbf{M}}^{(t)} \right\|^2 \\
& \quad + \frac{24\eta^2L^2\rho^2}{\lambda} + \frac{12\eta^2\delta^2}{\lambda} + 12\eta^2(1-\lambda)(\sigma^2 + 2L^2\rho^2)
\end{aligned} \tag{23}$$

In the above bound on the consensus error, we have a momentum error term $\mathbb{E} \left\| \mathbf{M}^{(t)} - \bar{\mathbf{M}}^{(t)} \right\|^2$. We present the following lemma to provide an upper bound on this error:

Lemma 7 Given Assumptions 1-3, the sequence of iterates generated by Q-SADDLe for $\frac{\beta}{1-\beta} \leq \frac{\lambda}{21}$,

$$\begin{aligned} & \frac{6\eta^2\beta^2}{n\lambda(1-\mu)(1-\beta)} \mathbb{E} \|\mathbf{M}^{t+1} - \bar{\mathbf{M}}^{t+1}\|^2 \leq \left(\frac{6\eta^2\beta^2}{n\lambda(1-\mu)(1-\beta)} - \frac{6\eta^2\beta^2}{n\lambda} \right) \mathbb{E} \|\mathbf{M}^{(t)} - \bar{\mathbf{M}}^{(t)}\|^2 \\ & + \frac{\lambda}{8n} \mathbb{E} \|\mathbf{X}^{(t)} - \bar{\mathbf{X}}^{(t)}\|^2 + \frac{\lambda\eta^2\delta^2}{8} + \left(\frac{3(1-\beta)}{(1-\mu)} + \frac{1}{2} \right) \frac{\lambda\eta^2L^2\rho^2}{4} + \frac{\lambda\eta^2\sigma^2(1-\beta)}{8(1-\mu)}. \end{aligned}$$

Proof: Starting from the update (8), we have:

$$\begin{aligned} & \frac{1}{n} \mathbb{E} \left\| \mathbf{M}^{(t+1)} - \bar{\mathbf{M}}^{(t+1)} \right\|^2 = \frac{1}{n} \mathbb{E} \left\| (\mu\mathbf{I} + (1-\mu)\beta\mathbf{W}) (\mathbf{M}^{(t)} - \bar{\mathbf{M}}^{(t)}) + (1-\mu)\mathbf{W}(\tilde{\mathbf{G}}^{(t)} \right. \\ & \left. - \bar{\mathbf{G}}^{(t)}) + \frac{1-\mu}{\eta} (\mathbf{I} - \mathbf{W})\mathbf{X}^{(t)} \right\|^2 = \frac{1}{n} \mathbb{E} \left\| (\mu\mathbf{I} + (1-\mu)\beta\mathbf{W}) (\mathbf{M}^{(t)} - \bar{\mathbf{M}}^{(t)}) + \right. \\ & \left. \frac{1-\mu}{\eta} (\mathbf{I} - \mathbf{W})\mathbf{X}^{(t)} + (1-\mu)\mathbf{W}(\mathbb{E}[\tilde{\mathbf{G}}^{(t)}] - \mathbb{E}[\bar{\mathbf{G}}^{(t)}]) \right\|^2 \\ & + \frac{1}{n} \mathbb{E} \left\| (1-\mu)\mathbf{W} \left(\tilde{\mathbf{G}}^{(t)} - \mathbb{E}[\tilde{\mathbf{G}}^{(t)}] - (\bar{\mathbf{G}}^{(t)} - \mathbb{E}[\bar{\mathbf{G}}^{(t)}]) \right) \right\|^2 \\ & \stackrel{a}{\leq} \frac{1}{n} \mathbb{E} \left\| (\mu\mathbf{I} + (1-\mu)\beta\mathbf{W}) (\mathbf{M}^{(t)} - \bar{\mathbf{M}}^{(t)}) + \frac{1-\mu}{\eta} (\mathbf{I} - \mathbf{W})\mathbf{X}^{(t)} + (1-\mu)\mathbf{W}(\mathbb{E}[\tilde{\mathbf{G}}^{(t)}] - \mathbb{E}[\bar{\mathbf{G}}^{(t)}]) \right\|^2 \\ & + 4(3\sigma^2 + 6L^2\rho^2) \stackrel{b}{\leq} \frac{1}{n} \left(1 + \frac{(1-\mu)(1-\beta)}{1-(1-\mu)(1-\beta)} \right) \mathbb{E} \left\| (\mu\mathbf{I} + (1-\mu)\beta\mathbf{W}) (\mathbf{M}^{(t)} - \bar{\mathbf{M}}^{(t)}) \right\|^2 \\ & + 12\sigma^2 + 24L^2\rho^2 + \frac{1}{n} \left(1 + \frac{1-(1-\mu)(1-\beta)}{(1-\mu)(1-\beta)} \right) \mathbb{E} \left\| \frac{1-\mu}{\eta} (\mathbf{I} - \mathbf{W})\mathbf{X}^{(t)} + (1-\mu)\mathbf{W}(\mathbb{E}[\tilde{\mathbf{G}}^{(t)}] - \mathbb{E}[\bar{\mathbf{G}}^{(t)}]) \right\|^2. \end{aligned} \tag{24}$$

(a) follows from Lemma 3, and (b) follows from the inequality $\|x_i + x_j\|^2 \leq (1+a)\|x_i\|^2 + (1+\frac{1}{a})\|x_j\|^2$ for any $a > 0$. Since $\mathbf{W} < \mathbf{I}$, we have $(\mu\mathbf{I} + (1-\mu)\beta\mathbf{W}) < (\mu + (1-\mu)\beta)\mathbf{I} = (1 - (1-\beta)(1-\mu))\mathbf{I}$. Further, we have $\mathbf{I} - \mathbf{W} < 2\mathbf{I}$ [34]. With these observations:

$$\begin{aligned} & \frac{1}{n} \mathbb{E} \left\| \mathbf{M}^{(t+1)} - \bar{\mathbf{M}}^{(t+1)} \right\|^2 \\ & \leq \frac{1}{n} \left(1 + \frac{(1-\mu)(1-\beta)}{1-(1-\mu)(1-\beta)} \right) \mathbb{E} \left\| (1 - (1-\mu)(1-\beta)) (\mathbf{M}^{(t)} - \bar{\mathbf{M}}^{(t)}) \right\|^2 + 12\sigma^2 + 24L^2\rho^2 \\ & + \frac{1}{n} \left(1 + \frac{1-(1-\mu)(1-\beta)}{(1-\mu)(1-\beta)} \right) \mathbb{E} \left\| \frac{1-\mu}{\eta} (\mathbf{I} - \mathbf{W})\mathbf{X}^{(t)} + (1-\mu)\mathbf{W}(\mathbb{E}[\tilde{\mathbf{G}}^{(t)}] - \mathbb{E}[\bar{\mathbf{G}}^{(t)}]) \right\|^2 \\ & \leq \frac{1}{n} (1 - (1-\mu)(1-\beta)) \mathbb{E} \left\| \mathbf{M}^{(t)} - \bar{\mathbf{M}}^{(t)} \right\|^2 + 12\sigma^2 + 24L^2\rho^2 \\ & + \frac{1}{(1-\mu)(1-\beta)n} \mathbb{E} \left\| \frac{1-\mu}{\eta} (\mathbf{I} - \mathbf{W})\mathbf{X}^{(t)} + (1-\mu)\mathbf{W}(\mathbb{E}[\tilde{\mathbf{G}}^{(t)}] - \mathbb{E}[\bar{\mathbf{G}}^{(t)}]) \right\|^2 \\ & \leq \frac{1}{n} (1 - (1-\mu)(1-\beta)) \mathbb{E} \left\| \mathbf{M}^{(t)} - \bar{\mathbf{M}}^{(t)} \right\|^2 + 12\sigma^2 + 24L^2\rho^2 + \frac{4(1-\mu)}{(1-\beta)n\eta^2} \mathbb{E} \left\| \mathbf{X}^{(t)} - \bar{\mathbf{X}}^{(t)} \right\|^2 \\ & + \frac{2(1-\mu)}{(1-\beta)n} \mathbb{E} \left\| \mathbb{E}[\tilde{\mathbf{G}}^{(t)}] - \mathbb{E}[\bar{\mathbf{G}}^{(t)}] \right\|^2. \end{aligned} \tag{25}$$

Substituting equation 21 in the above equation:

$$\begin{aligned}
& \frac{1}{n} \mathbb{E} \left\| \mathbf{M}^{(t+1)} - \bar{\mathbf{M}}^{(t+1)} \right\|^2 \leq \frac{1}{n} (1 - (1 - \mu)(1 - \beta)) \mathbb{E} \left\| \mathbf{M}^{(t)} - \bar{\mathbf{M}}^{(t)} \right\|^2 + 12\sigma^2 + 24L^2\rho^2 \\
& + \frac{4(1 - \mu)}{(1 - \beta)n\eta^2} \mathbb{E} \left\| \mathbf{X}^{(t)} - \bar{\mathbf{X}}^{(t)} \right\|^2 + \frac{8(1 - \mu)L^2}{(1 - \beta)n} \left(\sum_{i=1}^n \mathbb{E} \left\| \mathbf{x}_i^{(t)} - \bar{\mathbf{x}}^{(t)} \right\|^2 \right) + \frac{8(1 - \mu)L^2\rho^2}{(1 - \beta)} \\
& + \frac{4\delta^2(1 - \mu)}{(1 - \beta)} \leq \frac{1}{n} (1 - (1 - \mu)(1 - \beta)) \mathbb{E} \left\| \mathbf{M}^{(t)} - \bar{\mathbf{M}}^{(t)} \right\|^2 + 12\sigma^2 + 24L^2\rho^2 \\
& + \frac{4(1 - \mu)(1 + 2\eta^2L^2)}{(1 - \beta)n\eta^2} \mathbb{E} \left\| \mathbf{X}^{(t)} - \bar{\mathbf{X}}^{(t)} \right\|^2 + \frac{8(1 - \mu)L^2\rho^2}{(1 - \beta)} + \frac{4\delta^2(1 - \mu)}{(1 - \beta)}
\end{aligned} \tag{26}$$

Multiplying both sides by $\frac{6\eta^2\beta^2}{\lambda(1-\mu)(1-\beta)}$ yields

$$\begin{aligned}
& \frac{6\eta^2\beta^2}{\lambda n(1 - \mu)(1 - \beta)} \mathbb{E} \left\| \mathbf{M}^{(t+1)} - \bar{\mathbf{M}}^{(t+1)} \right\|^2 \leq \frac{6\eta^2\beta^2}{\lambda n} \left(\frac{1}{(1 - \mu)(1 - \beta)} - 1 \right) \mathbb{E} \left\| \mathbf{M}^{(t)} - \bar{\mathbf{M}}^{(t)} \right\|^2 \\
& + \left(\frac{24\beta^2(1 + 2\eta^2L^2)}{n\lambda(1 - \beta)^2} \right) \mathbb{E} \left\| \mathbf{X}^{(t)} - \bar{\mathbf{X}}^{(t)} \right\|^2 + \frac{72\eta^2\beta^2\sigma^2}{\lambda(1 - \mu)(1 - \beta)} + \frac{144\eta^2\beta^2L^2\rho^2}{\lambda(1 - \mu)(1 - \beta)} \\
& + \frac{48L^2\rho^2\eta^2\beta^2}{\lambda(1 - \beta)^2} + \frac{24\eta^2\beta^2\delta^2}{\lambda(1 - \beta)^2} \stackrel{a}{\leq} \frac{6\eta^2\beta^2}{\lambda n} \left(\frac{1}{(1 - \mu)(1 - \beta)} - 1 \right) \mathbb{E} \left\| \mathbf{M}^{(t)} - \bar{\mathbf{M}}^{(t)} \right\|^2 \\
& + \frac{\lambda}{8n} \mathbb{E} \left\| \mathbf{X}^{(t)} - \bar{\mathbf{X}}^{(t)} \right\|^2 + \frac{\lambda\eta^2\sigma^2(1 - \beta)}{6(1 - \mu)} + \left(\frac{(1 - \beta)}{3(1 - \mu)} + \frac{1}{9} \right) \lambda\eta^2L^2\rho^2 + \frac{\lambda\eta^2\delta^2}{18}
\end{aligned} \tag{27}$$

(a) follows from our assumption that the momentum parameter satisfies $\frac{\beta}{1-\beta} \leq \frac{\lambda}{21}$ and $\eta \leq \frac{1}{7L}$.

Adding the results of Lemma 6 and 7 and simplifying the coefficients, we describe the progress made in each gossip averaging consensus round:

$$\begin{aligned}
& \frac{1}{n} \mathbb{E} \left\| \mathbf{X}^{t+1} - \bar{\mathbf{X}}^{t+1} \right\|^2 + \frac{6\eta^2\beta^2}{n\lambda(1 - \mu)(1 - \beta)} \mathbb{E} \left\| \mathbf{M}^{t+1} - \bar{\mathbf{M}}^{t+1} \right\|^2 \\
& \leq \frac{1 - \lambda/8}{n} \mathbb{E} \left\| \mathbf{X}^t - \bar{\mathbf{X}}^t \right\|^2 + \frac{6\eta^2\beta^2}{n\lambda(1 - \mu)(1 - \beta)} \mathbb{E} \left\| \mathbf{M}^t - \bar{\mathbf{M}}^t \right\|^2 + \frac{13\eta^2\delta^2}{\lambda} \\
& + \frac{12\eta^2\sigma^2(2 - \beta - \mu)}{(1 - \mu)\lambda} + \frac{49\eta^2L^2\rho^2(2 - \beta - \mu)}{(1 - \mu)\lambda}
\end{aligned} \tag{28}$$

A.1 Proof for Theorem 1

We start with the following property for a L -smooth function $f(\mathbf{x})$:

$$\begin{aligned}
& \mathbb{E}f(\mathbf{z}^{(t+1)}) \leq \mathbb{E}f(\mathbf{z}^{(t)}) + \mathbb{E} \left\langle \nabla f(\mathbf{z}^{(t)}), \mathbf{z}^{(t+1)} - \mathbf{z}^{(t)} \right\rangle + \frac{L}{2} \mathbb{E} \left\| \mathbf{z}^{(t+1)} - \mathbf{z}^{(t)} \right\|^2 \\
& = \mathbb{E}f(\mathbf{z}^{(t)}) - \underbrace{\tilde{\eta} \mathbb{E} \left\langle \nabla f(\mathbf{z}^{(t)}), \frac{1}{n} \sum_{i=1}^n \nabla f_i(\mathbf{x}_i^t + \xi_i^t) \right\rangle}_I + \frac{L}{2} \underbrace{\mathbb{E} \left\| \mathbf{z}^{(t+1)} - \mathbf{z}^{(t)} \right\|^2}_{II}
\end{aligned} \tag{29}$$

We first focus on finding an upper bound for I :

$$I : \frac{1}{2} \left(\mathbb{E} \left\| \nabla f(\mathbf{z}^t) \right\|^2 + \mathbb{E} \left\| \frac{1}{n} \sum_{i=1}^n \nabla f_i(\mathbf{x}_i^t + \xi_i^t) \right\|^2 \right) - \frac{1}{2} \underbrace{\left(\mathbb{E} \left\| \nabla f(\mathbf{z}^t) - \frac{1}{n} \sum_{i=1}^n \nabla f_i(\mathbf{x}_i^t + \xi_i^t) \right\|^2 \right)}_{\star} \tag{30}$$

To bound \star :

$$\star : \left(\mathbb{E} \left\| \frac{1}{n} \sum_{i=1}^n \nabla f_i(\mathbf{z}^t) - \frac{1}{n} \sum_{i=1}^n \nabla f_i(\mathbf{x}_i^t + \xi_i^t) \right\|^2 \right) \leq \frac{1}{n} \sum_{i=1}^n \mathbb{E} \|\nabla f_i(\mathbf{z}^t) - \nabla f_i(\mathbf{x}_i^t + \xi_i^t)\|^2 \quad (31)$$

Substituting equation 31 in 30:

$$I \geq \frac{1}{2} \left(\mathbb{E} \|\nabla f(\mathbf{z}^t)\|^2 + \mathbb{E} \left\| \frac{1}{n} \sum_{i=1}^n \nabla f_i(\mathbf{x}_i^t + \xi_i^t) \right\|^2 \right) - \frac{1}{2n} \sum_{i=1}^n \mathbb{E} \|\nabla f_i(\mathbf{z}^t) - \nabla f_i(\mathbf{x}_i^t + \xi_i^t)\|^2 \quad (32)$$

Now, we find an upper bound for II :

$$\mathbb{E} \|\mathbf{z}^{(t+1)} - \mathbf{z}^{(t)}\|^2 = \tilde{\eta}^2 \mathbb{E} \|\bar{\mathbf{g}}\|^2 \stackrel{a}{\leq} \tilde{\eta}^2 \left(\frac{3\sigma^2}{n} + \frac{6L^2\rho^2}{n} + \mathbb{E} \left\| \frac{1}{n} \sum_{i=1}^n \nabla f_i(\mathbf{x}_i^t + \xi_i^t) \right\|^2 \right) \quad (33)$$

Here, (a) is the result of Lemma 4. Putting equation 32 and 33 in 29:

$$\begin{aligned} \mathbb{E} f(\mathbf{z}^{(t+1)}) &\leq \mathbb{E} f(\mathbf{z}^{(t)}) - \frac{\tilde{\eta}}{2} \mathbb{E} \|\nabla f(\mathbf{z}^t)\|^2 - \frac{\tilde{\eta}}{2} \mathbb{E} \left\| \frac{1}{n} \sum_{i=1}^n \nabla f_i(\mathbf{x}_i^t + \xi_i^t) \right\|^2 + \\ &+ \frac{\tilde{\eta}}{2n} \sum_{i=1}^n \mathbb{E} \|\nabla f_i(\mathbf{z}^t) - \nabla f_i(\mathbf{x}_i^t + \xi_i^t)\|^2 + \frac{\tilde{\eta}^2 L}{2} \left(\frac{3\sigma^2}{n} + \frac{6L^2\rho^2}{n} + \mathbb{E} \left\| \frac{1}{n} \sum_{i=1}^n \nabla f_i(\mathbf{x}_i^t + \xi_i^t) \right\|^2 \right) \end{aligned} \quad (34)$$

Rearranging the above terms we get:

$$\begin{aligned} \mathbb{E} f(\mathbf{z}^{(t+1)}) &\leq \mathbb{E} f(\mathbf{z}^{(t)}) - \frac{\tilde{\eta}}{2} \mathbb{E} \|\nabla f(\mathbf{z}^t)\|^2 + \left(\frac{\tilde{\eta}^2 L}{2} - \frac{\tilde{\eta}}{2} \right) \mathbb{E} \left\| \frac{1}{n} \sum_{i=1}^n \nabla f_i(\mathbf{x}_i^t + \xi_i^t) \right\|^2 + \\ &\frac{\tilde{\eta}}{2n} \sum_{i=1}^n \mathbb{E} \|\nabla f_i(\mathbf{z}^t) - \nabla f_i(\mathbf{x}_i^t + \xi_i^t)\|^2 + \frac{3\tilde{\eta}^2 L^3 \rho^2}{n} + \frac{3\tilde{\eta}^2 L \sigma^2}{2n} \leq \mathbb{E} f(\mathbf{z}^{(t)}) - \frac{\tilde{\eta}}{4} \mathbb{E} \|\nabla f(\bar{\mathbf{x}}^t)\|^2 \\ &+ \underbrace{\frac{\tilde{\eta}}{2} \mathbb{E} \|\nabla f(\mathbf{z}^t) - \nabla f(\bar{\mathbf{x}}^t)\|^2 + \frac{\tilde{\eta}}{2n} \sum_{i=1}^n \mathbb{E} \|\nabla f_i(\mathbf{z}^t) - \nabla f_i(\mathbf{x}_i^t + \xi_i^t)\|^2}_{\star} \\ &+ \left(\frac{\tilde{\eta}^2 L}{2} - \frac{\tilde{\eta}}{2} \right) \mathbb{E} \left\| \frac{1}{n} \sum_{i=1}^n \nabla f_i(\mathbf{x}_i^t + \xi_i^t) \right\|^2 + \frac{3\tilde{\eta}^2 L^3 \rho^2}{n} + \frac{3\tilde{\eta}^2 L \sigma^2}{2n} \end{aligned} \quad (35)$$

Now we simplify \star :

$$\begin{aligned} \star &: \frac{\tilde{\eta}}{2n} \sum_{i=1}^n \mathbb{E} \|\nabla f_i(\mathbf{z}^t) - \nabla f_i(\bar{\mathbf{x}}^t)\|^2 + \frac{\tilde{\eta}}{2n} \sum_{i=1}^n \mathbb{E} \|\nabla f_i(\mathbf{z}^t) - \nabla f_i(\mathbf{x}_i^t + \xi_i^t)\|^2 \\ &\leq \frac{\tilde{\eta}}{2n} \sum_{i=1}^n \mathbb{E} \|\nabla f_i(\mathbf{z}^t) - \nabla f_i(\bar{\mathbf{x}}^t)\|^2 + \frac{\tilde{\eta}}{n} \sum_{i=1}^n \mathbb{E} \|\nabla f_i(\mathbf{z}^t) - \nabla f_i(\bar{\mathbf{x}}^t)\|^2 \\ &+ \frac{\tilde{\eta}}{n} \sum_{i=1}^n \mathbb{E} \|\nabla f_i(\bar{\mathbf{x}}^t) - \nabla f_i(\mathbf{x}_i^t + \xi_i^t)\|^2 = \frac{3\tilde{\eta}}{2n} \sum_{i=1}^n \mathbb{E} \|\nabla f_i(\mathbf{z}^t) - \nabla f_i(\bar{\mathbf{x}}^t)\|^2 \\ &+ \frac{\tilde{\eta}}{n} \sum_{i=1}^n \mathbb{E} \|\nabla f_i(\bar{\mathbf{x}}^t) - \nabla f_i(\mathbf{x}_i^t + \xi_i^t)\|^2 \end{aligned} \quad (36)$$

Putting this back into equation 35:

$$\begin{aligned} \mathbb{E}f(\mathbf{z}^{(t+1)}) &\leq \mathbb{E}f(\mathbf{z}^{(t)}) - \frac{\tilde{\eta}}{4}\mathbb{E}\|\nabla f(\bar{\mathbf{x}}^t)\|^2 + \left(\frac{\tilde{\eta}^2 L}{2} - \frac{\tilde{\eta}}{2}\right)\mathbb{E}\left\|\frac{1}{n}\sum_{i=1}^n \nabla f_i(\mathbf{x}_i^t + \xi_i^t)\right\|^2 + \\ &\frac{3\tilde{\eta}}{2}\sum_{i=1}^n \mathbb{E}\|\nabla f_i(\mathbf{z}^t) - \nabla f_i(\bar{\mathbf{x}}^t)\|^2 + \frac{\tilde{\eta}}{n}\sum_{i=1}^n \mathbb{E}\|\nabla f_i(\bar{\mathbf{x}}^t) - \nabla f_i(\mathbf{x}_i^t + \xi_i^t)\|^2 + \frac{3\tilde{\eta}^2 L^3 \rho^2}{n} + \\ &\frac{3\tilde{\eta}^2 L \sigma^2}{2n} \end{aligned} \quad (37)$$

Using our assumption $\tilde{\eta} \leq \frac{1}{4L}$ and Assumption 1, we have:

$$\begin{aligned} \mathbb{E}f(\mathbf{z}^{(t+1)}) &\leq \mathbb{E}f(\mathbf{z}^{(t)}) - \frac{\tilde{\eta}}{4}\mathbb{E}\|\nabla f(\bar{\mathbf{x}}^t)\|^2 - \frac{\tilde{\eta}}{4}\mathbb{E}\left\|\frac{1}{n}\sum_{i=1}^n \nabla f_i(\mathbf{x}_i^t + \xi_i^t)\right\|^2 + \\ &\frac{3\tilde{\eta}L^2}{2}\sum_{i=1}^n \mathbb{E}\|\mathbf{z}^t - \bar{\mathbf{x}}^t\|^2 + \frac{\tilde{\eta}L^2}{n}\sum_{i=1}^n \mathbb{E}\|\bar{\mathbf{x}}^t - \mathbf{x}_i^t - \xi_i^t\|^2 + \frac{3\tilde{\eta}^2 L^3 \rho^2}{n} + \frac{3\tilde{\eta}^2 L \sigma^2}{2n} \stackrel{a}{\leq} \mathbb{E}f(\mathbf{z}^{(t)}) \\ &- \frac{\tilde{\eta}}{4}\mathbb{E}\|\nabla f(\bar{\mathbf{x}}^t)\|^2 - \frac{\tilde{\eta}}{4}\mathbb{E}\left\|\frac{1}{n}\sum_{i=1}^n \nabla f_i(\mathbf{x}_i^t + \xi_i^t)\right\|^2 + \frac{3\tilde{\eta}L^2}{2}\sum_{i=1}^n \mathbb{E}\|\mathbf{z}^t - \bar{\mathbf{x}}^t\|^2 + \\ &\frac{2\tilde{\eta}L^2}{n}\sum_{i=1}^n \mathbb{E}\|\bar{\mathbf{x}}^t - \mathbf{x}_i^t\|^2 + 2\tilde{\eta}L^2 \rho^2 + \frac{3\tilde{\eta}^2 L^3 \rho^2}{n} + \frac{3\tilde{\eta}^2 L \sigma^2}{2n} \end{aligned} \quad (38)$$

(a) follows from the perturbation ξ_i being bounded by the perturbation radius ρ .

Now we see that the terms $\|\mathbf{z}^{(t)} - \bar{\mathbf{x}}^{(t)}\|^2$ and $\|\bar{\mathbf{x}}^t - \mathbf{x}_i^t\|^2$, which we bound in Lemma 5 and 6 respectively, appear in the above equation. We start by Lemma 5, and scale both sides by $\frac{3L^2\tilde{\eta}}{2(1-\mu)(1-\beta)}$:

$$\begin{aligned} \frac{3L^2\tilde{\eta}}{2(1-\mu)(1-\beta)}\mathbb{E}\|\mathbf{e}^{(t+1)}\|^2 &\leq \left(\frac{3L^2\tilde{\eta}}{2(1-\mu)(1-\beta)} - \frac{3L^2\tilde{\eta}}{2}\right)\mathbb{E}\|\mathbf{e}^{(t)}\|^2 \\ &+ \frac{3L^2\tilde{\eta}^3\beta^2}{(1-\beta)^2(1-\mu)^2}\mathbb{E}\|\mathbb{E}_t[\bar{\mathbf{g}}^{(t)}]\|^2 + \frac{9L^2\tilde{\eta}^3\beta^2\sigma^2}{2(1-\mu)(1-\beta)} + \frac{9L^4\tilde{\eta}^3\beta^2\rho^2}{(1-\mu)(1-\beta)} \end{aligned} \quad (39)$$

Next, we take the total consensus change from equation 28, and scale it with $\frac{16L^2\tilde{\eta}}{\lambda}$:

$$\begin{aligned} &\frac{16L^2\tilde{\eta}}{\lambda n}\mathbb{E}\|\mathbf{X}^{t+1} - \bar{\mathbf{X}}^{t+1}\|^2 + \frac{96\tilde{\eta}^3\beta^2(1-\beta)}{n\lambda^2(1-\mu)}\mathbb{E}\|\mathbf{M}^{t+1} - \bar{\mathbf{M}}^{t+1}\|^2 \\ &\leq \frac{16L^2\tilde{\eta}}{\lambda n}\mathbb{E}\|\mathbf{X}^t - \bar{\mathbf{X}}^t\|^2 + \frac{96\tilde{\eta}^3\beta^2(1-\beta)}{n\lambda^2(1-\mu)}\mathbb{E}\|\mathbf{M}^t - \bar{\mathbf{M}}^t\|^2 \\ &- \frac{2L^2\tilde{\eta}}{n}\mathbb{E}\|\mathbf{X}^t - \bar{\mathbf{X}}^t\|^2 + \frac{208L^2\tilde{\eta}^3(1-\beta)^2\delta^2}{\lambda^2} + \frac{192L^2\tilde{\eta}^3(2-\beta-\mu)(1-\beta)^2\sigma^2}{(1-\mu)\lambda^2} \\ &+ \frac{784L^4\tilde{\eta}^3(1-\beta)^2(2-\beta-\mu)\rho^2}{(1-\mu)\lambda^2} \end{aligned} \quad (40)$$

Through equation 39 and 40, we define another sequence $\phi^t \geq 0$ such that $\phi^0 = \mathbb{E}[f(\bar{\mathbf{x}}^0) - f^*]$:

$$\phi^t : \frac{16L^2\tilde{\eta}}{\lambda n}\mathbb{E}\|\mathbf{X}^t - \bar{\mathbf{X}}^t\|^2 + \frac{96L^2\tilde{\eta}^3\beta^2(1-\beta)}{n\lambda^2(1-\mu)}\mathbb{E}\|\mathbf{M}^t - \bar{\mathbf{M}}^t\|^2 + \frac{3L^2\tilde{\eta}}{2(1-\mu)(1-\beta)}\mathbb{E}\|\mathbf{e}^{(t)}\|^2 + \mathbb{E}[f(\bar{\mathbf{x}}^t) - f^*]$$

Adding the right hand sides of equation 38, 39 and 40, and bounding ϕ^{t+1} in terms of ϕ^t :

$$\begin{aligned}
\phi^{t+1} &\leq \phi^t - \frac{\tilde{\eta}}{4} \left\| \nabla f(\bar{\mathbf{x}}^{(t)}) \right\|^2 + \left(\frac{3L^2\tilde{\eta}^3\beta^2}{(1-\beta)^2(1-\mu)^2} - \frac{\tilde{\eta}}{4} \right) \mathbb{E} \left\| \frac{1}{n} \sum_{i=1}^n \nabla f_i(\mathbf{x}_i^t + \xi_i^t) \right\|^2 + 2\tilde{\eta}L^2\rho^2 \\
&+ \frac{3\tilde{\eta}^2L^3\rho^2}{n} + \frac{3\tilde{\eta}^2L\sigma^2}{2n} + \frac{9L^2\tilde{\eta}^3\beta^2\sigma^2}{2(1-\mu)(1-\beta)} + \frac{9L^4\tilde{\eta}^3\beta^2\rho^2}{(1-\mu)(1-\beta)} + \frac{208L^2\tilde{\eta}^3(1-\beta)^2\delta^2}{\lambda^2} \\
&+ \frac{192L^2\tilde{\eta}^3(2-\beta-\mu)(1-\beta)^2\sigma^2}{(1-\mu)\lambda^2} + \frac{784L^4\tilde{\eta}^3(1-\beta)^2(2-\beta-\mu)\rho^2}{(1-\mu)\lambda^2}
\end{aligned} \tag{41}$$

Simplifying the above equation by rearranging terms and approximating some coefficients:

$$\begin{aligned}
\left\| \nabla f(\bar{\mathbf{x}}^{(t)}) \right\|^2 &\leq \frac{4}{\tilde{\eta}} (\phi^t - \phi^{t+1}) + \left(\frac{12L^2\tilde{\eta}^2\beta^2}{(1-\beta)^2(1-\mu)^2} - 1 \right) \mathbb{E} \left\| \frac{1}{n} \sum_{i=1}^n \nabla f_i(\mathbf{x}_i^t + \xi_i^t) \right\|^2 + \\
&\underbrace{\left(\frac{6\tilde{\eta}L}{n} + 18\tilde{\eta}^2L^2C_2 + \frac{768\tilde{\eta}^2L^2C_1}{\lambda^2} \right)}_{C_\sigma} \sigma^2 + \underbrace{\left(\frac{832L^2\tilde{\eta}^2(1-\beta)^2}{\lambda^2} \right)}_{C_\delta} \delta^2 \\
&+ \underbrace{\left(8L^2 + \frac{12\tilde{\eta}L^3}{n} + 36\tilde{\eta}^2L^4C_2 + \frac{3136L^4\tilde{\eta}^2C_1}{\lambda^2} \right)}_{C_\rho} \rho^2
\end{aligned} \tag{42}$$

Here, $C_1 = \frac{(2-\beta-\mu)(1-\beta)^2}{(1-\mu)}$ and $C_2 = \frac{\beta^2}{(1-\mu)(1-\beta)}$.

For $\frac{12L^2\tilde{\eta}^2\beta^2}{(1-\beta)^2(1-\mu)^2} - 1 \leq 0$:

$$\left\| \nabla f(\bar{\mathbf{x}}^{(t)}) \right\|^2 \leq \frac{4}{\tilde{\eta}} (\phi^t - \phi^{t+1}) + C_\sigma\sigma^2 + C_\delta\delta^2 + C_\rho\rho^2 \tag{43}$$

Averaging over T , we have:

$$\frac{1}{T} \sum_{t=0}^{T-1} \mathbb{E} \left\| \nabla f(\bar{\mathbf{x}}^{(t)}) \right\|^2 \leq \frac{4}{\tilde{\eta}T} (f(\bar{\mathbf{x}}^0) - f^*) + C_\sigma\sigma^2 + C_\delta\delta^2 + C_\rho\rho^2 \tag{44}$$

A.2 Proof for Corollary 2

To find the convergence rate with a learning rate $\eta = \mathcal{O}\left(\sqrt{\frac{n}{T}}\right)$ and perturbation radius $\rho = \mathcal{O}\left(\sqrt{\frac{1}{T}}\right)$, we find the order of all the terms in equation 44:

- $\frac{4}{\tilde{\eta}T} (f(\bar{\mathbf{x}}^0) - f^*) = \mathcal{O}\left(\frac{1}{\sqrt{nT}}\right)$
- $C_\sigma\sigma^2 = \mathcal{O}\left(\frac{\eta}{n} + \eta^2\right) = \mathcal{O}\left(\frac{1}{\sqrt{nT}} + \frac{n}{T}\right)$
- $C_\delta\delta^2 = \mathcal{O}\left(\eta^2\right) = \mathcal{O}\left(\frac{n}{T}\right)$
- $C_\rho\rho^2 = \mathcal{O}\left(\rho^2 + \frac{\eta\rho^2}{n} + \eta^2\rho^2\right) = \mathcal{O}\left(\frac{1}{T} + \frac{1}{n^{1/2}T^{3/2}} + \frac{n}{T^2}\right)$

Adding all the terms and ignoring n in higher order terms:

$$\frac{1}{T} \sum_{t=0}^{T-1} \mathbb{E} \left\| \nabla f(\bar{\mathbf{x}}^{(t)}) \right\|^2 \leq \mathcal{O}\left(\frac{1}{\sqrt{nT}} + \frac{1}{T} + \frac{1}{T^{3/2}} + \frac{1}{T^2}\right) \tag{45}$$

This implies that when T is sufficiently large, Q-SADDLe converges at the rate of $\mathcal{O}\left(\frac{1}{\sqrt{nT}}\right)$.

A.3 Condition on Learning Rate η and Momentum Coefficient β

In Lemma 6, we assume $\eta \leq \frac{\lambda}{10L}$ and in Lemma 7, we assume $\eta \leq \frac{1}{7L}$. Combining both bounds results in $\eta \leq \min(\frac{1}{7L}, \frac{\lambda}{10L}) \leq \min(\frac{1}{7L}, \frac{\lambda}{7L}) \leq \frac{\lambda}{7L}$. In Theorem 1 proof, we assume $\eta \leq \frac{(1-\beta)}{4L}$ to simplify equation 37. Further to simplify equation 42, we have the following upper bound on η :

$$\begin{aligned} \frac{12L^2\tilde{\eta}^2\beta^2}{(1-\beta)^2(1-\mu)^2} - 1 &\leq 0 \\ 12L^2\tilde{\eta}^2\beta^2 - (1-\beta)^2(1-\mu)^2 &\leq 0 \\ \eta &\leq \frac{(1-\beta)^2(1-\mu)}{\sqrt{12L}\beta} \end{aligned} \quad (46)$$

Combining all the above mentioned bounds, we can describe $\eta \leq \min\left(\frac{\lambda}{7L}, \frac{1-\beta}{4L}, \frac{(1-\beta)^2(1-\mu)}{\sqrt{12L}\beta}\right)$.

Similarly, for momentum coefficient β , we assume $\frac{\beta}{1-\beta} \leq \frac{\lambda}{21}$ in Lemma 7. Note that we don't abide by these constraints and still achieve competitive performance for our results in Section 6.2 and Appendix C.

B Algorithmic Details

B.1 Background

To highlight that SADDLe can improve the generalization and communication efficiency of existing decentralized algorithms, we choose two state-of-the-art techniques for our evaluation: Quasi-Global Momentum (QGM) [34] and Neighborhood Gradient Mean (NGM) [2]. QGM improves the performance of D-PSGD [33] without introducing any extra communication. However, as shown in our results in Section 6.2, it performs poorly with extreme data heterogeneity. To achieve competitive performance with higher degrees of non-IIDness, NGM proposes to boost the performance through cross-gradients, which require 2x communication (i.e., an extra round of communication) as compared to D-PSGD [33].

Quasi-Global Momentum (QGM): The authors in QGM [34] show that local momentum acceleration is hindered by data heterogeneity. Inspired by this, QGM updates the momentum buffer by computing the difference between two consecutive models \mathbf{x}_i^{t+1} and \mathbf{x}_i^t to approximate the global optimization direction locally. The following equation illustrates the update rule for QGM:

$$\text{QGM: } \mathbf{x}_i^{t+1} = \sum_{j \in \mathcal{N}(i)} w_{ij} [\mathbf{x}_j^t - \eta(\mathbf{g}_j^t + \beta \mathbf{m}_j^{t-1})]; \quad \mathbf{m}_i^t = \mu \mathbf{m}_i^{t-1} + (1-\mu) \frac{\mathbf{x}_i^t - \mathbf{x}_i^{(t+1)}}{\eta}. \quad (47)$$

Neighborhood Gradient Mean (NGM): NGM [2] modifies the local gradient update with the aid of self and cross-gradients. The self-gradients are computed at each agent through its model parameters and the local dataset. The data variant cross-gradients are derivatives of the local model with respect to the dataset of neighbors. These gradients are obtained through an additional round of communication. The update rule for NGM is shown in equation 48, where each gradient update \mathbf{g}_j^t is a weighted average of the self and received cross-gradients.

$$\text{NGM: } \mathbf{x}_i^{t+1} = \sum_{j \in \mathcal{N}(i)} w_{ij} \mathbf{x}_j^t - \eta \mathbf{g}_j^t; \quad \mathbf{g}_j^t = \sum_{j \in \mathcal{N}(i)} w_{ij} \nabla F_j(\mathbf{x}_i^t; d_j^t). \quad (48)$$

B.2 N-SADDLe and Comp N-SADDLe

Algorithm 3 highlights the difference between NGM and N-SADDLe. Specifically, N-SADDLe computes SAM-based gradient updates for self and cross gradients (lines 4 and 8). Similarly, please refer to Algorithm 4 to understand the difference between the compressed versions of NGM and N-SADDLe (i.e., Comp NGM and Comp N-SADDLe). The error between the original gradients and their compressed version is added as feedback to the gradients before compressing them in the next iteration (lines 5,6,13, and 14 in Algorithm 4).

Algorithm 3 NGM vs N-SADDLe

Input: Each agent $i \in [1, n]$ initializes model weights \mathbf{x}_i , step size η , momentum coefficient β , averaging rate γ , mixing matrix $\mathbf{W} = [w_{ij}]_{i,j \in [1,n]}$, and I_{ij} are elements of $n \times n$ identity matrix, $\mathcal{N}(i)$ represents neighbors of i including itself.

procedure TRAIN(\cdot) $\forall i$

1. **for** $t = 1, 2, \dots, T$ **do**
 2. $d_i^t \sim D^i$
 3. $\mathbf{g}_{ii}^t = \nabla F_i(\mathbf{x}_i^t; d_i^t)$
 4. $\tilde{\mathbf{g}}_{ii}^t = \nabla F_i(\mathbf{x}_i^t + \xi(\mathbf{x}_i^t); d_i^t)$, where $\xi(\mathbf{x}_i^t) = \rho \frac{\mathbf{g}_{ii}^t}{\|\mathbf{g}_{ii}^t\|}$
 5. SENDRECEIVE(\mathbf{x}_i^t)
 6. **for** each neighbor $j \in \{\mathcal{N}(i) - i\}$ **do**
 7. $\mathbf{g}_{ji}^t = \nabla F_i(\mathbf{x}_j^t; d_i^t)$
 8. $\tilde{\mathbf{g}}_{ji}^t = \nabla F_i(\mathbf{x}_j^t + \xi(\mathbf{x}_j^t); d_i^t)$, where $\xi(\mathbf{x}_j^t) = \rho \frac{\mathbf{g}_{ji}^t}{\|\mathbf{g}_{ji}^t\|}$
 9. SENDRECEIVE (\mathbf{g}_{ji}^t) ($\tilde{\mathbf{g}}_{ji}^t$)
 10. **end**
 11. $\mathbf{g}_i^t = \sum_{j \in \mathcal{N}(i)} w_{ij} \mathbf{g}_{ij}^t$
 12. $\mathbf{m}_i^t = \beta \mathbf{m}_i^{(t-1)} + \mathbf{g}_i^t$
 13. $\tilde{\mathbf{g}}_i^t = \sum_{j \in \mathcal{N}(i)} w_{ij} \tilde{\mathbf{g}}_{ij}^t$
 14. $\tilde{\mathbf{m}}_i^t = \beta \mathbf{m}_i^{(t-1)} + \tilde{\mathbf{g}}_i^t$
 15. $\mathbf{x}_i^{(t+1/2)} = \mathbf{x}_i^t - \eta \mathbf{m}_i^t$
 16. $\mathbf{x}_i^{(t+1)} = \mathbf{x}_i^{(t+1/2)} + \gamma \sum_{j \in \mathcal{N}(i)} (w_{ij} - I_{ij}) \mathbf{x}_j^t$
 17. **end**
 - return** \mathbf{x}_i^T
-

C Additional Results

C.1 SADDLe with DPSGD

A natural question that arises is, does SADDLe improve the performance of DPSGD[33] in the presence of data heterogeneity? Note that DPSGD assumes the data distribution to be IID and has been shown to incur significant performance drop with non-IID data [34]. Algorithm 5 shows the difference between DPSGD and D-SADDLe, a version incorporating SAM-based updates within DPSGD. D-SADDLe leads to an average improvement of 10% and 5.4% over DPSGD for CIFAR-10 and CIFAR-100 datasets, respectively, as shown in Table 5.

Table 5: Test accuracy of DPSGD and D-SADDLe evaluated on CIFAR-10 and CIFAR-100 over ResNet-20, distributed with different degrees of heterogeneity over ring topologies.

Agents	Method	CIFAR-10		CIFAR-100	
		$\alpha = 0.01$	$\alpha = 0.001$	$\alpha = 0.01$	$\alpha = 0.001$
5	DPSGD (IID)	91.05 \pm 0.06		64.47 \pm 0.48	
	DPSGD	82.15 \pm 3.25	80.54 \pm 4.36	47.30 \pm 4.92	45.54 \pm 0.71
	<i>D-SADDLe (ours)</i>	85.38 \pm 0.84	84.94 \pm 0.31	54.35 \pm 0.48	54.30 \pm 0.50
10	DPSGD (IID)	90.46 \pm 0.33		62.73 \pm 1.03	
	DPSGD	49.17 \pm 17.38	40.74 \pm 2.62	31.66 \pm 0.84	29.79 \pm 1.30
	<i>D-SADDLe (ours)</i>	64.18 \pm 5.63	61.30 \pm 0.79	37.49 \pm 0.59	35.31 \pm 0.77
20	DPSGD (IID)	89.46 \pm 0.02		59.61 \pm 1.15	
	DPSGD	40.49 \pm 3.06	36.13 \pm 5.67	24.45 \pm 0.51	21.58 \pm 1.00
	<i>D-SADDLe (ours)</i>	52.14 \pm 2.02	47.06 \pm 2.35	26.39 \pm 0.17	24.92 \pm 0.62

Algorithm 4 Comp NGM vs Comp N-SADDLe

Input: Each agent i initializes model weights \mathbf{x}_i , step size η , averaging rate γ , mixing matrix $\mathbf{W} = [w_{ij}]_{i,j \in [1,n]}$, $Q(\cdot)$ is the compression operator, $\mathcal{N}(i)$ represents neighbors of i including itself.

procedure TRAIN() $\forall i$

1. **for** $t=1, 2, \dots, T$ **do**
 2. $d_i^t \sim D_i$
 3. $\mathbf{g}_{ii}^t = \nabla F_i(\mathbf{x}_i^t; d_i^t)$
 4. $\tilde{\mathbf{g}}_{ii}^t = \nabla F_i(\mathbf{x}_i^t + \xi(\mathbf{x}_i^t); d_i^t)$, where $\xi(\mathbf{x}_i^t) = \rho \frac{\mathbf{g}_{ii}^t}{\|\mathbf{g}_{ii}^t\|}$
 5. $\mathbf{p}_{ii}^t = \mathbf{g}_{ii}^t + \mathbf{e}_{ii}^t$
 6. $\tilde{\mathbf{p}}_{ii}^t = \tilde{\mathbf{g}}_{ii}^t + \mathbf{e}_{ii}^t$
 7. $\delta_{ii}^t = Q(\mathbf{p}_{ii}^t)$
 8. $\mathbf{e}_{ii}^{t+1} = \mathbf{p}_{ii}^t - \delta_{ii}^t$
 9. SENDRECEIVE(\mathbf{x}_i^t)
 10. **for** each neighbor $j \in \{N(i) - i\}$ **do**
 11. $\mathbf{g}_{ji}^t = \nabla F_i(\mathbf{x}_j^t; d_i^t)$
 12. $\tilde{\mathbf{g}}_{ji}^t = \nabla F_i(\mathbf{x}_j^t + \xi(\mathbf{x}_j^t); d_i^t)$, where $\xi(\mathbf{x}_j^t) = \rho \frac{\mathbf{g}_{ji}^t}{\|\mathbf{g}_{ji}^t\|}$
 13. $\mathbf{p}_{ji}^t = \mathbf{g}_{ji}^t + \mathbf{e}_{ji}^t$
 14. $\tilde{\mathbf{p}}_{ji}^t = \tilde{\mathbf{g}}_{ji}^t + \mathbf{e}_{ji}^t$
 15. $\delta_{ji}^t = Q(\mathbf{p}_{ji}^t)$
 16. $\mathbf{e}_{ji}^{t+1} = \mathbf{p}_{ji}^t - \delta_{ji}^t$
 17. SENDRECEIVE(δ_{ji}^t)
 18. **end**
 19. **end**
 20. $\mathbf{g}_i^t = \sum_{j \in \mathcal{N}(i)} w_{ij} \delta_{ij}^t$
 21. $\mathbf{m}_i^t = \beta \mathbf{m}_i^{(t-1)} + \mathbf{g}_i^t$
 22. $\mathbf{x}_i^{(t+1/2)} = \mathbf{x}_i^t - \eta \mathbf{m}_i^t$
 23. $\mathbf{x}_i^{(t+1)} = \mathbf{x}_i^{(t+1/2)} + \gamma \sum_{j \in \mathcal{N}(i)} (w_{ij} - I_{ij}) \mathbf{x}_j^t$
 24. **end**
- return** \mathbf{x}_i^T
-

Algorithm 5 DPSGD vs D-SADDLe

Input: Each agent $i \in [1, n]$ initializes model weights $\mathbf{x}_i^{(0)}$, learning rate η , perturbation radius ρ , and mixing matrix $\mathbf{W} = [w_{ij}]_{i,j \in [1,n]}$, $\mathcal{N}(i)$ represents neighbors of i including itself.

procedure TRAIN() $\forall i$

1. **for** $t=0, 1, \dots, T-1$ **do**
 2. $d_i^k \sim D_i$
 3. $\mathbf{g}_i^t = \nabla F_i(d_i^t; \mathbf{x}_i^t)$
 4. $\tilde{\mathbf{g}}_i^t = \nabla F_i(\mathbf{x}_i^t + \xi(\mathbf{x}_i^t); d_i^t)$, where $\xi(\mathbf{x}_i^t) = \rho \frac{\mathbf{g}_i^t}{\|\mathbf{g}_i^t\|}$
 5. $\mathbf{x}_i^{(t+\frac{1}{2})} = \mathbf{x}_i^t - \eta \mathbf{g}_i^t$
 6. $\tilde{\mathbf{x}}_i^{(t+\frac{1}{2})} = \mathbf{x}_i^t - \eta \tilde{\mathbf{g}}_i^t$
 7. SENDRECEIVE($\mathbf{x}_i^{(t+\frac{1}{2})}$)
 8. $\mathbf{x}_i^{(t+1)} = \sum_{j \in \mathcal{N}_i} w_{ij} \mathbf{x}_j^{t+\frac{1}{2}}$
- return**
-

C.2 Results with Top-k Sparsification

We present results for QGM and Q-SADDLe with Top-30% Sparsification-based compressor in Table 6. Note that Top-30% implies that only the top 30% of model updates for each layer are communicated to the peers. As shown in Table 6, QGM performs poorly in the presence of compression, with a significant drop of $\sim 5 - 57\%$, and the training even diverges for some cases. In contrast, Q-SADDLe is much more stable, with an accuracy drop of $\sim 0.6 - 18.5\%$ with compression.

Table 6: Test accuracy (Acc) and accuracy drop (Drop) of QGM and Q-SADDLe with Sparsification (top-30%) based compression evaluated on CIFAR-10 distributed over ring topologies. \star indicates 1 out of 3 runs diverged.

Agents	Comp	Method	CIFAR-10			
			$\alpha = 0.01$		$\alpha = 0.001$	
			Acc (%)	Drop(%)	Acc (%)	Drop(%)
5	✓	QGM	83.58 \pm 2.96	4.86	67.04 \pm 9.76	21.68
	✓	<i>Q-SADDLe (ours)</i>	90.01 \pm 0.38	0.65	89.49 \pm 0.38	1.18
10	✓	QGM	52.23 \star	25.18	23.00 \pm 1.96	56.48
	✓	<i>Q-SADDLe (ours)</i>	80.34 \pm 5.56	7.38	71.01 \pm 3.75	15.32
20	✓	QGM	62.90 \pm 5.89	9.3	32.92 \pm 9.25	29.56
	✓	<i>Q-SADDLe (ours)</i>	71.96 \pm 2.51	6.45	64.31 \pm 2.14	18.50

C.3 Results for Torus Topology

We present additional results on torus topology with 20 and 40 agents in Table 7. Each agent has 4 peers/neighbors; hence, the torus has higher connectivity than the ring. Q-SADDLe and N-SADDLe achieve 16.5% and 0.8% better accuracy than QGM and NGM, respectively. In the presence of communication compression, Q-SADDLe incurs a $\sim 3\%$ drop, while QGM suffers a significant accuracy drop of 9.6%. Interestingly, both NGM and N-SADDLe nearly retain their accuracy even in the presence of compression.

Table 7: Test accuracy of different decentralized algorithms evaluated on CIFAR-10, distributed with $\alpha = 0.001$ over torus topology.

Agents	Comp	Method	Accuracy(%)
20		QGM	56.07 \pm 3.88
	✓	QGM	47.62 \pm 6.75
		<i>Q-SADDLe (ours)</i>	77.10 \pm 1.18
	✓	<i>Q-SADDLe (ours)</i>	74.50 \pm 1.31
		NGM	88.18 \pm 0.17
	✓	NGM	87.71 \pm 0.54
40		<i>N-SADDLe (ours)</i>	89.21 \pm 0.26
	✓	<i>N-SADDLe (ours)</i>	89.30 \pm 0.36
		QGM	57.96 \pm 3.90
	✓	QGM	47.08 \pm 7.72
		<i>Q-SADDLe (ours)</i>	70.05 \pm 3.35
	✓	<i>Q-SADDLe (ours)</i>	64.84 \pm 2.46
40		NGM	86.00 \pm 0.34
	✓	NGM	86.30 \pm 0.52
		<i>N-SADDLe (ours)</i>	86.67 \pm 0.32
	✓	<i>N-SADDLe (ours)</i>	87.00 \pm 0.18

C.4 Compression Error and Gradient Norms for N-SADDLe

Recall that the expectation of compression error for a compression operator $Q(\cdot)$ has the following upper bound:

$$\mathbb{E}_Q \|Q(\theta) - \theta\|^2 \leq (1 - \delta) \|\theta\|^2, \text{ where } \delta > 0 \quad (49)$$

For NGM and N-SADDLe, θ corresponds to the gradients \mathbf{g}_i and $\tilde{\mathbf{g}}_i$ respectively. In Figure 5, we compare the compression error ($\|Q(\theta) - \theta\|$) and gradient norms for NGM and N-SADDLe with

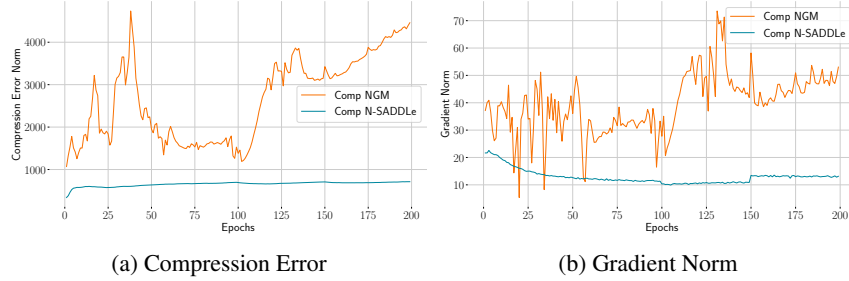


Figure 5: Impact of flatness on (a) Compression Error and (b) Gradient Norm for ResNet-20 trained on CIFAR-10 distributed in a non-IID manner across a 10 agent ring topology.

a 1-bit Sign SGD-based compression scheme. Clearly, N-SADDLe leads to a lower compression error, as well as lower gradient norms throughout the training. Here, we plot the sum of layer-wise compression errors and the sum of gradient norms for each layer in the ResNet-20 model. Like Q-SADDLe, the bound in Equation 49 is tighter for N-SADDLe than NGM. Note that our observation regarding lower gradient norms in the presence of SAM aligns with the fact that SAM optimization is a special form of penalizing the gradient norm [49].

C.5 Stochastic Quantization for NGM and N-SADDLe

The main paper uses Sign SGD [24] compression scheme with NGM and N-SADDLe since it has been shown to perform better than stochastic quantization for extreme compression [26, 24]. However, to demonstrate the generalizability of our approach, we present results on 2-bit stochastic quantization in Table 8. NGM incurs an average drop of 4.4%, while N-SADDLe incurs only a 1.2% average accuracy drop in the presence of this compression scheme.

Table 8: Test accuracy (Acc) and accuracy drop (Drop) of NGM and N-SADDLe with 2-bit quantization compression scheme [3] evaluated on CIFAR-10, with $\alpha = 0.01, 0.001$.

Agents	Comp	Method	CIFAR-10 (ResNet-20)			
			$\alpha = 0.01$		$\alpha = 0.001$	
			Acc (%)	Drop(%)	Acc (%)	Drop(%)
5	✓	NGM	87.38 ± 2.01	3.49	87.27 ± 0.56	3.46
	✓	<i>N-SADDLe (ours)</i>	91.35 ± 0.17	0.61	91.18 ± 0.25	0.51
10	✓	NGM	79.89 ± 8.74	5.19	79.20 ± 3.05	4.23
	✓	<i>N-SADDLe (ours)</i>	87.25 ± 1.65	1.18	85.70 ± 1.15	1.59
20	✓	NGM	81.87 ± 1.17	2.97	76.68 ± 0.95	6.90
	✓	<i>N-SADDLe (ours)</i>	84.25 ± 0.17	2.01	85.09 ± 0.31	1.52

C.6 Loss Landscape Visualization

To visualize the loss landscape, we randomly sample two directions through orthogonal Gaussian perturbations [32] and plot the loss for ResNet-20 trained with CIFAR-10 distributed across 10 nodes with $\alpha = 0.001$. As shown in Figure 6, we observe that Q-SADDLe and Comp Q-SADDLe have much smoother loss landscapes than QGM and Comp QGM. The compressed counterparts of QGM and Q-SADDLe are relatively sharper than their respective full communication versions. This is intuitively expected since communication compression leads agents to receive less information from their neighbors, resulting in more reliance on local updates. This can exacerbate over-fitting in the presence of data heterogeneity. We observe similar trends for NGM, N-SADDLe, and their compressed versions as shown in Figure 7.

C.7 Communication Cost

This section presents the exact amount of data transmitted (in Gigabytes) during training (refer Tables 9, 10, 11, 12 and 13).

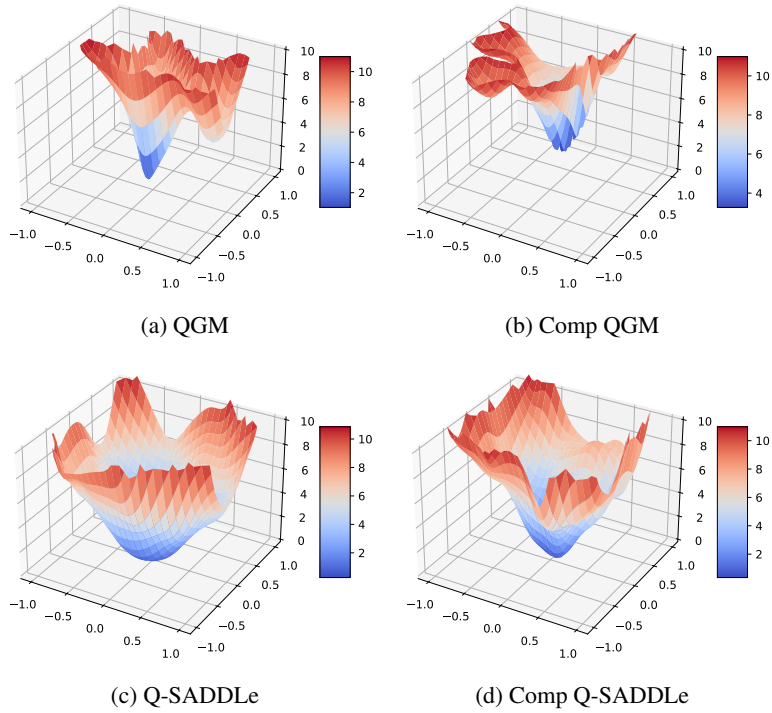


Figure 6: Visualization of the loss landscape for ResNet-20 trained on the CIFAR-10 dataset distributed across a 10 agent ring topology with $\alpha = 0.001$.

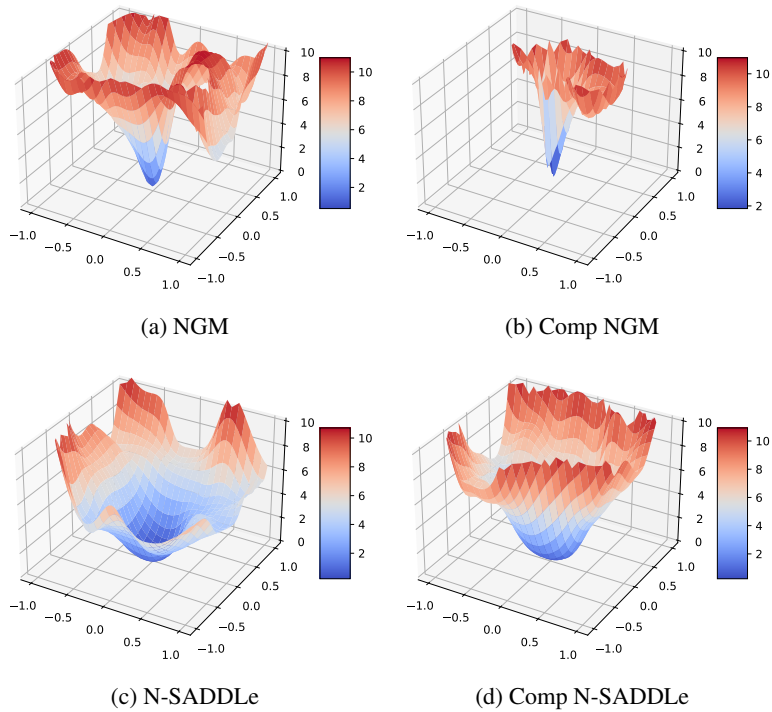


Figure 7: Visualization of the loss landscape for ResNet-20 trained on the CIFAR-10 dataset distributed across a 10 agent ring topology with $\alpha = 0.001$.

Table 9: Communication costs per agent (in GBs) for experiments in Table 1. The results presented in Table 1 use a stochastic quantization-based compression scheme with 8 bits for communication compression, leading to a $4\times$ reduction in communication cost.

Agents	Comp	Method	CIFAR-10	CIFAR-100
5	✓	QGM and Q -SADDLe	136.45	111.32
		QGM and Q -SADDLe	34.11	27.83
10	✓	QGM and Q -SADDLe	68.44	55.66
		QGM and Q -SADDLe	17.11	13.91
20	✓	QGM and Q -SADDLe	34.43	27.83
		QGM and Q -SADDLe	8.60	6.95
40	✓	QGM and Q -SADDLe	17.43	14.02
		QGM and Q -SADDLe	4.35	3.50

Table 10: Communication costs per agent (in GBs) for experiments in Table 6. Table 6 uses a top-30% compression scheme, leading to a $2.2\times$ reduction in communication cost.

Agents	Comp	Method	CIFAR-10
5	✓	QGM and Q -SADDLe	61.38
10	✓	QGM and Q -SADDLe	30.78
20	✓	QGM and Q -SADDLe	15.49

Table 11: Communication costs per agent (in GBs) for experiments in Table 2. The results presented in Table 2 use a stochastic quantization-based compression scheme with 10 bits for communication compression, leading to a $3.2\times$ reduction in communication cost.

Agents	Comp	Method	Imagenette
5	✓	QGM and Q -SADDLe	110.23
		QGM and Q -SADDLe	34.44
10	✓	QGM and Q -SADDLe	55.10
		QGM and Q -SADDLe	17.21

Table 12: Communication costs per agent (in GBs) for experiments in Table 3. The results presented in Table 3 use 1-bit Sign SGD for communication compression, leading to a $32\times$ reduction in the communication cost for the second round and a total of $1.94\times$ reduction in the entire communication cost.

Agents	Comp	Method	CIFAR-10	CIFAR-100
5	✓	NGM and N -SADDLe	272.91	222.65
		NGM and N -SADDLe	140.67	114.76
10	✓	NGM and N -SADDLe	136.89	111.32
		NGM and N -SADDLe	70.56	57.38
20	✓	NGM and N -SADDLe	68.88	55.66
		NGM and N -SADDLe	35.50	28.69

Table 13: Communication costs per agent (in GBs) for experiments in Table 4. The results presented in Table 4 use 1-bit Sign SGD for communication compression, leading to a $32\times$ reduction in the communication cost for the second round and a total of $1.94\times$ reduction in the entire communication cost.

Agents	Comp	Method	Imagenette	ImageNet
10	✓	NGM and N -SADDLe	110.25	22466.30
		NGM and N -SADDLe	56.82	11580.56

D Decentralized Learning Setup

All our experiments were conducted on a system with 4 NVIDIA A40 GPUs, each with 48GB GDDR6. We report the test accuracy of the consensus model averaged over three randomly chosen seeds. This section details graph topologies, data heterogeneity, datasets, models, and training hyper-parameters.

D.1 Visualization of Graph Topologies

Figure 8 shows the ring and torus topologies used in this paper. As can be seen in this figure, the ring has 2 peers per agent, while the torus has 4. For the results in the main paper, we focus on ring, one of the most sparsely connected graph topologies. Furthermore, to show the generalizability of our approach, we present results on torus topology in Table 7.

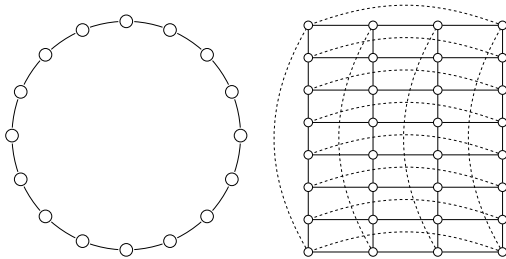


Figure 8: Ring Graph (left), and Torus Graph (right).

D.2 Visualization of Non-IID Data

Figure 9 illustrates the number of samples from each class allocated to each agent for the 2 different Dirichlet distribution α values used in our work. It is clear that $\alpha = 0.001$ corresponds to the most extreme form of data heterogeneity, i.e. samples from only 1 class per agent. Note that this level of non-IIDness has been used in CGA [13] and NGM [2] to evaluate the performance. $\alpha = 0.01$ has been used in QGM [34] and is relatively mild, with most agents accessing samples from 2 different classes (and some even from 4 classes).

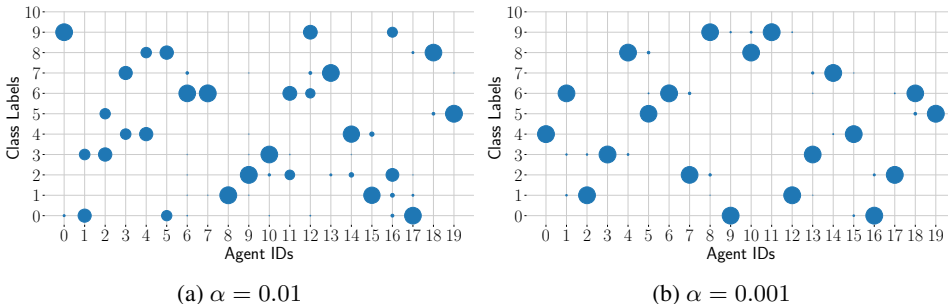


Figure 9: Visualization of the number of samples from each class allocated to each agent for different Dirichlet distribution α values on the CIFAR-10 dataset.

D.3 Datasets

CIFAR-10: CIFAR-10 [30] is an image classification dataset with 10 classes. Each class has 5000 training samples and 1000 test samples (i.e., a total of 50,000 training and 10,000 test samples). These image samples have 32×32 resolution, with 3 input channels.

CIFAR-100: CIFAR-100 [30] is an image classification dataset with 100 classes. Each class has 500 training samples and 100 test samples (i.e., a total of 50,000 training and 10,000 test samples). CIFAR-100 is a more challenging dataset than CIFAR-10 since the number of samples per class is much lesser, and there is a wider variety of classes to learn.

ImageNet: ImageNet [11] is one of the most challenging large-scale image classification datasets. It has 1000 classes, with 1300 training samples for each class. Each image sample has a resolution of 224×224 . The terms of access (and license details) are available at <https://image-net.org/download.php>.

Imagenette: Imagenette [20] is a 10-class subset of the ImageNet dataset with image samples having 3 input channels and a resolution of 224×224 . There are about 9469 training samples and 3925 test

samples in total. Our experiments use a resized version of these samples with a resolution of 32×32 . We use this dataset through <https://github.com/fastai/imagenette> (Apache License 2.0).

D.4 Model Architectures

All the models use Evonorm [35] as it has been shown to be better suited for non-IID data [17]. We use the standard ResNet-20 and ResNet-18 [16] architectures with 0.27M and 11M trainable parameters, respectively. For MobileNet-V2, we use the standard architecture used for the CIFAR-10 dataset with 2.3M parameters [39].

D.5 Hyper-parameters

This section presents the hyper-parameters for results presented in Section 6.2 and Appendix C. All our experiments were run for three randomly chosen seeds. We decay the learning rate by $10 \times$ after 50% and 75% of the training for all experiments except for ImageNet results in Table 4 and Figure 2. For ImageNet, we decay the learning rate by $10 \times$ after 33%, 67%, and 90% of the training. For Figure 2, we use the StepLR scheduler, where the learning rate decays by 0.981 after every epoch. We use a Nesterov momentum of 0.9 for all our experiments except DPSGD and D-SADDLe in Table 5, for which we use no momentum. Note that similar to QGM [34], we keep $\mu = \beta$ for all our experiments. We also use a weight decay of $1e-4$ for all the presented experiments. Please refer to Table 14 for the learning rate, perturbation radius, number of epochs, and batch size per agent for all the experiments in this paper. For a fair comparison, we ensure that all the techniques utilize the same set of hyper-parameters.

We tune the global averaging rate γ through a grid search over $\gamma = \{0.01, 0.1, 0.2, \dots, 1.0\}$ and present the fine-tuned γ used for experiments in Tables 3, 4 and 8 in Table 15. For results in Tables 1, 2 and 5, we use $\gamma = 1.0$ for all the experiments. For Top-30% Sparsification results shown in Table 6, we use $\gamma = 0.4$. For our experiments on torus topology in Table 7, we use an averaging rate of 0.5.

Table 14: Learning rate (η), the perturbation radius (ρ) (where applicable), batch size per agent, and the number of epochs for all the experiments for QGM, Q-SADDLe, NGM, N-SADDLe, and their compressed versions across various datasets.

Dataset	CIFAR-10	CIFAR-100	Imagenette	ImageNet
Learning Rate (η)	0.1	0.1	0.01	0.01
Perturbation Radius (ρ)	0.1	0.05	0.01	0.05
Epochs	200	100	100	60
Batch-Size/Agent	32	20	32	64

Table 15: Global averaging rate (γ) for our experiments in Table 3, 4 and 8.

Method	Non-IID Level (α)	CIFAR-10	CIFAR-100	Imagenette	ImageNet
NGM	0.01	1.0	1.0	0.5	1.0
	0.001	1.0	1.0	0.5	1.0
Comp NGM	0.01	0.5	0.5	0.1	0.5
	0.001	0.5	0.5	0.5	0.5
N-SADDLe	0.01	1.0	1.0	0.5	1.0
	0.001	1.0	1.0	0.5	1.0
Comp N-SADDLe	0.01	0.5	0.5	0.1	1.0
	0.001	0.5	0.5	0.5	1.0